Self-destructive altruism in a synthetic developmental program enables complex feedstock utilization

Robert Egbert[1], Leandra Brettner[2], David Zong[2] and Eric Klavins[1]

1 University of Washington, Electrical Engineering (Seattle, WA, USA);
2 University of Washington, Bioengineering (Seattle, WA, USA)

Abstract

Stochastic differentiation and programmed cell death are core developmental processes in microbes, driving diverse altruistic behaviors that promote cooperative behaviors. Utilizing cell death in developmental programs requires control over differentiation rates to balance cell proliferation against the utility of sacrifice. However, the regulatory networks that control these behaviors are often complex and have yet to be successfully harnessed as biotechnology. Here, we engineered a synthetic developmental gene network that couples stochastic differentiation with programmed cell death to implement a two-member division of labor. Progenitor cellobiose consumer cells were engineered to grow on cellobiose and differentiate at a controlled rate into self-destructive altruists that release a cellulase enzyme payload through autolysis to create a developmental *Escherichia coli* consortium that utilizes cellulose for growth. A population dynamics model predicted fitness in cellulose based on parameter estimates of modular circuit components, including increased growth observed with altruist cells modified to export a multi-cellulase cocktail that liberated 14-23% of the available carbon. An inevitable consequence of engineering developmental behaviors is the emergence of cheaters that undermine cooperation. We observed cheater phenotypes for consumers and altruists, identified modes of evolutionary escape and identified the relationship between mutation rates and circuit longevity, a requirement for extending developmental programs to complex environments. This work introduces the developmental program as a new tool for synthetic circuit design, demonstrates the utility of population dynamics models in this setting and provides a testbed for probing the evolutionary biology of self-destructive altruism.

Introduction

Compartmentalization of function across differentiated cell types was essential to the emergence of complexity in biological systems. Organogenesis in plants and animals[1], schizogamy in polychaete worms[2] and germ-soma differentiation in *Volvox* algae[3] are clear examples of these divisions of labor. Microbial developmental programs utilize stochastic differentiation and programmed cell death as vital components of population fitness[4]. Selection for programmed cell death has been proposed to drive complex behaviors that delay commitment to costly cell fate decisions[5], enable adaptation to environmental fluctuations[6], eliminate competitor species[7], reinforce biofilm structure[8] and promote colonization of hostile environments[9]. These behaviors represent divisions of labor between subpopulations of progenitor (germ) cells that propagate the species and sacrificial (soma) cells that provide a public good. Many aspects of the emergence of multi-cellular cooperation and the genetic circuits that control its complexity remain unclear. Limited understanding of the architectures and stimuli that control developmental gene networks limits efforts to repurpose them to engineer cell behaviors.

Current engineering paradigms of DNA-encoded logic and feedback control circuits in cells fail to encompass the full suite of behaviors desired to advance the fields of bioprocessing, bioremediation and cell-based therapeutics. Protein production and release is challenging[10,11], often requiring protein or molecule-specific pumps. Deterministic autolysis allows release of protein payloads[12] but limits applications that may require consistent, dosed delivery. A major challenge to engineering synthetic microbial consortia is the control of population distributions for complex traits. While syntrophic interactions in defined communities may address some of these needs, they may not be sustainable in unconstrained nutrient or complex microbial environments. Synthetic developmental programs could address these challenges, enabling approaches to create, and regenerate, microbial communities seeded by individual cells that cooperatively implement complex behaviors.

SDAc as a developmental program

Here we present a synthetic developmental program that implements a germ-soma division of labor to cooperatively digest cellulose. The program links a synthetic differentiation circuit with autolysis-mediated enzymatic payload delivery, balancing the rates of stochastic differentiation and programmed cell death to drive population growth. We constructed a genetic circuit to create cellobiose consumer cells that produce a sub-population of self-destructive altruists at a controlled rate to enable utilization of cellulose as a sole carbon source through extracellular release of cellulase payloads (Figure 1a). We refer to the system as SDAc, short for self-destructive altruism with a cellulase payload. We implemented SDAc in *Escherichia coli* by engineering a native operon to efficiently utilize cellobiose, introducing a genetic toggle switch tuned to function as a differentiation controller, and constructing a cellulase-lysis payload module to execute the altruist behavior (Figure 1b). We used dynamical systems modeling to identify core parameters of the gene network and demonstrated control over the circuit behavior by fine-tuning each parameter.

SDAc network architecture

Using multiplexed mutagenesis and selection, we isolated a strain with a growth rate in cellobiose that is 63% its growth rate in glucose. Though *E. coli* does not natively digest cellobiose, we modified the *chb* operon in a recombinogenic MG1655 derivative[13] by replacing the native chitobiose-regulated promoter with a strong constitutive promoter[14]. We further improved growth on cellobiose by subjecting the constitutive *chb* variant to multiple cycles of single-strand DNA multiplexed recombineering targeting the *chb* genes and selected for cellobiose utilization in minimal cellobiose media (Supplementary Figure 1). We identified the variant with the highest growth rate, DL069, as a *chbR* deletion mutant.

To control differentiation rate, we constructed and sampled from a library of mutual inhibition toggle switch variants that exhibit regular stochastic state transitions. While genetic toggle switches are often designed to function as bistable memory devices[15], a quasi-steady state can be achieved by properly balancing expression levels of the repressor proteins[16]. Simple sequence repeats embedded in the ribosome binding site (rbSSR) allow predictable modulation of translation initiation rate to tune the balance between transcriptional repressors[17], which for this circuit are LacI and TetR.

We engineered altruist payload delivery by constructing a cellulase and lysis gene cassette. The operon was designed to maximize production of the cellulase payload with an efficient ribosome binding site and a poly-

(AT) rbSSR to fine-tune lysis gene expression. Minimization of the fitness defects of self-destructive altruism dictates post-differentiation accumulation of the payload followed by autolysis. Colicin gene networks share this trait, using stochastic gene expression of colicin and lysis genes within subpopulations to deliver a toxin against ecological competitors[7,18]. We found that coupling the lysis gene from colicin E3 to the differentiation controller enabled stochastic state transitions and delayed lysis at the microcolony level, evidenced by post-differentiation accumulation of a GFP payload followed by autolysis (Figure 1c and Supplementary Movie).

Model description for self-destructive altruism with enzymatic payload

Analysis of a population dynamics model of SDAc behavior suggested optimal parameter regimes for cellulose utilization and guided implementation of the developmental circuit. Though we observed the requisite behaviors of differentiation, payload accumulation and autolytic release at the microcolony level, it was not clear what expression levels of circuit components would enable cooperative growth on cellulose. To reason about the functional parameter space for the SDAc circuit we developed a population dynamics model using a system of ordinary differential equations that maps core parameters to experimentally tunable features of the genetic circuit. The model species are consumers, altruists, cellulose feedstock, and cellulose-derived nutrients. These species and the associated kinetic parameters are described in Box 1.

The core tunable parameters for SDAc cellulose utilization are the growth rate on cellobiose, differentiation rate, lysis rate, and cellulase activity. Cells must utilize the hydrolysis products of the cellulase enzymes, significantly cellobiose. Minimal differentiation would limit growth via insufficient cellulase production, while excessive differentiation would incur unnecessary fitness defects for consumers or, at extreme rates, to population collapse. Low lysis rates would limit feedstock degradation through intracellular cellulase sequestration and excessive rates would reduce payload burst size due to premature lysis. High cellulase activity improves growth titer by reducing the population fraction of altruists required to deconstruct the feedstock. Ultimately, SDAc performance is constrained by the tunability of the circuit components and large regions of parameter space predict no growth on cellulose (Supplementary Figure 2).

SDAc parameter estimates through modular system decomposition

The modularity of synthetic gene circuits allowed us to decompose the system model and its experimental components to estimate core parameters and predict cellulose utilization for the full circuit. We developed the modules described in Box 1 to measure growth rate on cellobiose, differentiation rate, lysis rate, and cellulase activity, each drawing from a small part library to sample a range of parameters.

We experimentally tuned differentiation rate over an order of magnitude with a collection of autolysis deficient SDAc strains. Specifically, we used multiple poly-(T) rbSSR variants controlling TetR expression to modulate the differentiation rate from TetR-dominant consumers to LacI-dominant altruists deficient in autolysis (Figure 2a,b). We measured the population fraction of differentiated cells as a function of time using flow cytometry (Supplementary Figure 3) and fit a two-state, continuous growth model to the data for consumers transitioning to altruists at rate σ (Box1, Module ii). We found that the repeat length was inversely proportional to switching rate, supporting previous results for a different copy number plasmid[17] and resulting

in σ estimates ranging from $2.7\times10^{-2}\pm9.0\times10^{-3}\,h^{-1}$ for $(\mathrm{T})_{12}$ to $2.11\times10^{-1}\pm1.5\times10^{-2}\,h^{-1}$ for $(\mathrm{T})_{18}$ (Figure 2c, Supplementary Table 4).

Lysis rates were modulated over a four-fold range using expression variants of the colicin E3 lysis gene. Using intermediate differentiator $(\mathrm{T})_{16}$, we tested a set of poly-(AT) rbSSR variants to modulate lysis gene expression (Figure 2d,e). We used the same population fraction assay as for differentiation to fit a consumer growth and differentiation model that includes altruist lysis parameter ρ (Box1, Module iii). We measured lysis rates from $7.3\times10^{-2}\pm1.8\times10^{-2}\,h^{-1}$ for $(\mathrm{AT})_{11}$ to $1.9\times10^{-1}\pm2.5\times10^{-2}\,h^{-1}$ for $(\mathrm{AT})_{8}$ (Figure 2f, Supplementary Table 5). As predicted by the model, the differentiated fraction of each switch variant expressing an $(\mathrm{AT})_{8}$ lysis gene is lower than for the equivalent autolysis-deficient strain (Supplementary Figure 5). We found, however, that the lysis rate was well-correlated to the poly-(AT) (Supplementary Figure 6).

To estimate cellulase activity we quantified cellulose degradation from cell lysates of autolysis-deficient SDAc strains producing individual cellulases, observing hydrolysis rates over a five-fold range. We measured cellulose degradation and digestible nutrient release for three endoglucanases from two glycoside hydrolase (GH) families: CelD04[19] and BsCel5[20] from GH5; and CpCel9 from GH9[21]. We also measured the activity of multi-enzyme cocktails using each GH5 enzyme with CpCel9, combinations shown to have synergistic activities[22] (Figure 2f,g). We used Congo Red staining to observe cellulose degradation up to 23% (Supplementary Note 6) in M9 minimal phosphoric acid swollen cellulose (PASC) spiked with cell lysate and quantified cell growth on the resulting supernatant to estimate nutrient release of up to 14% of cellobiose equivalents (see Supplementary Figure 8, Supplementary Note 6). We used these cellulase activity measurements to fit a value for ω to the feedstock differential equation (Box 1, Module iv, Equation 3). Cellulase activity estimates range from $3.6\times10^{-13}\pm3.9\times10^{-13}$ CFU^{-1} mL for CpCel9 to $1.9\times10^{-12}\pm3.0\times10^{-13}$ CFU^{-1} mL for the BsCel5/CpCel9 cocktail (Figure 2i, Supplementary Table 7).

Full system performance & model predictability

To quantify the combined effects of SDAc differentiation and autolysis dynamics on feedstock degradation we measured cellulase activity on cellulose. Cellulose hydrolysis by individual colonies was measured by Congo Red clearing assays on agar plates supplemented with carboxymethylcellulose (Figure 3). We found that the clearing diameter for switch variants increased as a function of differentiation rate (Figure 3b). We observed no clearings for a control lacking cellulase. We also tested the effect of rbSSR lysis variants for cellulase CelD04 (Figure 3c,d) as well as for individual cellulases (Figure 3g,h) using the intermediate differentiator $(\mathrm{T})_{16}$. We found the GH5 cellulases generated larger clearings than CpCel9, consistent with the in vitro cellulase activity results.

Fine-tuning the differentiation, lysis and cellulase activity parameters is critical to realizing robust SDAc growth on cellulose as a sole carbon source. To determine fitness on cellulose and validate the full dynamics model (Box 1, module i), we measured viable cell counts in PASC for SDAc variants that span a range of values for each core parameter (Figure 3). We found optimal SDAc fitness at intermediate differentiation rates (Figure 3c), with efficient payload release (Figure 3f) and with high cellulase activity (Figure 3i), trends that are consistent with the naive model predictions in Supplementary Figure 2. Growth kinetics fits using parameter estimates from individual modules match observations for most variants, though the model

predicted longer lags for differentiation variant $(T)_{18}$ and failed to capture a late boost in cell density for the BsCel5-CpCel9 cellulase (Supplementary figure 8).

SDAc system cheaters

The full dynamics model of SDAc growth on cellulose predicts that high differentiation rates will lead to system collapse (Figure 3a), but does not account for mutational dynamics that could produce non-cooperative cheaters. Indeed, we found the SDAc system showed long-term functional instability for hyperdifferentiator switch variant $(T)_{18}$. We observed the instability in the cellobiose differentiation assay as two distinct, temporally separated steady-state altruist fractions, a result that was corroborated by two population growth rate regimes from the same assay (see Figure 4d,e). We also observed three distinct colony phenotypes after extended growth in PASC media (Figure 4a), further suggesting functional instability for extreme parameter values.

NEXT TWO NEED TO BE UPDATED BASED ON MODELING DATA

Application of all potential models incorporating cheater states suggests that two cheater phenotypes independently deficient in differentiation and lysis are necessary to observe the measured dynamics. Four potential models are possible for the cheater dynamics, each with multiple potential initial condition states. The models account for differentiation-deficient cheaters, lysis-deficient cheaters, both cheater types, or no observable cheater phenotypes (Figure 4b). For initial conditions, cheaters may arise from distinct mutation events during growth or be pre-existent in the culture and rise in population fraction once the majority of cells differentiate and lyse. We derived analytical solutions for each of these models, finding that the only models that support the observed data include both cheater states (Supplementary Note 10). These analytical solutions do not distinguish between initial conditions that require *de novo* mutagenesis or inocula that contain small mutant populations.

To examine the SDAc dynamics with cheaters, we developed a model that introduces new species for switch consumer cheaters (S) and or pseudo-altruist lysis cheaters (P) and their associated escape rates, χ_C and χ_A, respectively (Box 1, module iv). We applied the extended model to the differentiation and lysis data for cellobiose growth for hyperdifferentiator $(T)_{18}$ (Figure 4c). The model fit estimates consumer cell defections to switch cheats at a rate of $1.2\times10^{-5} \pm 9.8\times10^{-6}\ h^{-1}$ and the emergence of altruist cheats at a rate of $7.5\times10^{-5} \pm 3.5\times10^{-5}\ h^{-1}$. Using cheater parameters fit from hyperdifferentiator $(T)_{18}$, intermediate differentiator $(T)_{16}$ is also predicted to accumulate cheaters within the measurement interval, which fits the trend of the cellobiose switching data. When applying the same escape rates to the combined population growth rate for differentiation variants, we found the model predicted the observed growth rate dynamics for variants with high differentiation rates (Figure 4d). Further, using the cheater rate estimates into a modified PASC growth model that incorporates cheater dynamics improves the growth fit for the differentiation variants, in particular $(T)_{18}$ (Supplementary Figure 9e).

DNA sequencing of cheater isolates confirms genetic sources for both differentiation and lysis deficiencies (Figure 4e). We observed bright red colonies and bright green colonies – putative differentiation and lysis cheaters, respectively – media in addition to the expected mixed-color colony on solid media after growth in PASC. Sequence analysis of the differentiation plasmid from red escape colonies isolated from six replicate

cultures revealed mutations to two hypermutable loci with predictable effects (Supplementary Table 10): expansion or contraction of the tandem $(CTGG)_3$ mutational hotspot observed in four of six replicates should prevent altruist emergence through inactive, truncated Lac repressor[23]; deletions within the $(T)_{18}$ rbSSR controlling TetR expression (one of six replicates) should abolish differentiation by reducing σ; and a transposition event of IS2[24] (one of six replicates) internal to *lacI* should abolish state transition.

Sequence analysis of the payload delivery plasmid revealed transposition of IS1[25] between the cellulase and lysis genes in one of six sequenced replicates, likely disrupting operon expression (Supplementary Table 11). The majority of the altruist cheater colonies we sequenced had perfect sequencing reads in the payload delivery transcription unit, suggesting lysis evasion via mutations on the genome or elsewhere on the plasmids. Given that the lysis gene is sourced from a colicin plasmid found in natural *E. coli* populations, it is possible the MG1655 genome encodes evolutionary paths to lysis immunity.

Discussion

We have demonstrated a first-principles approach to construct simple developmental gene circuits for synthetic biology and implemented one developmental system to utilize the complex feedstock cellulose. In-depth system deconstruction and characterization enables model-guided optimization of system performance.

Due to the observed functional instability of some switch variants, the SDAc system likely suffers from a tragedy of the commons[26]. In well-mixed cellulose media, emergent cheaters fully benefit from the public good provided by the altruists. Further, due to the costs of switching and lysis, the cheaters can out-compete cooperators and sweep the population. In the absence of altruists, cellulose degradation ceases, resulting in population collapse. Previous work has shown that when the environment is organized spatially a communal benefit applies only to nearby, closely related cells who are likely fellow cooperators[27]. Cheaters are stranded with limited or no access to the shared resource. This phenomenon, attributed to kin selection, could preserve cooperative behavior for many more generations, potentially avoiding the functional instability currently observed in the system. Future work could elucidate the role of structured environments in this synthetic system to reduce the impact of cheaters or evolve more stable cooperator phenotypes.

While we only observed a high fraction of SDAc cheaters from hyperdifferentiation variant $(T)_{18}$, engineering developmental circuits for deployment in bioreactors or other complex environments would require long-term evolutionary stability to minimize cheaters and maintain engineered function. Interestingly, previous studies showed that *lacI* tandem repeat mutations occur at a rate > 10^{-6} per generation[23] and transposon insertion elements jump at rates of 10^{-6}-10^{-5} per generation[28], rates similar to our mutagenesis estimates, suggesting relatively simple modifications may considerably boost SDAc circuit longeivity. Some strategies to boost evolutionary stability include recoding the repeat region of *lacI*, replacing or introducing degeneracy into rbSSR sequences and porting the system to a low mutation rate strain missing insertion elements[29]. Further gains in system performance could be achieved by chromosomal integration of the SDAc network to prevent the fixation of mutant plasmids in the population[30] or plasmid loss. Finally, incorporating higher activity cellulase cocktails will reduce the evolutionary pressure for cheating by reducing the population fraction required for self-destructive altruism. Analysis of the cheater model suggests a reduction of each cheater

rate by 10-fold and 100-fold for intermediate differentiator $(T)_{16}$ would bring 39% and 81% increases in circuit stability, respectively, from 2.8 days to up to 5.1 days.

The division of labor system outlined here enables the construction of developmental programs that can perform complex tasks in engineered microbial communities and this work can be extended in many ways. Self-destructive altruism behavior could be triggered in response to nutrient depletion, or to deliver alternative public good payloads. Stochastic strategies could be employed with or without self-destructive altruism to seed multicellular developmental programs for distributed metabolic engineering[31], evolutionary engineering[32] or to control distributions of multiple cell types in microbial communities[33,34]. Tunable developmental programs could also be applied to better understand the emergence and persistence of extant developmental programs, replacing complex regulation with tunable differentiation dynamics.

Acknowledgements

The authors thank Ben Kerr for helpful discussions regarding evolutionary dynamics of self-destructive altruism and for the colicin E3 plasmid. They also thank Chris Takahashi for sharing strain CT009.

References

1. Weissman, I. L. Stem cells: units of development, units of regeneration, and units in evolution. *Cell* **100,** 157–168 (2000).
2. Franke, H.-D. Reproduction of the Syllidae (Annelida: Polychaeta). *Hydrobiologia* **402,** 39–55 (1999).
3. Prochnik, S. E. *et al.* Genomic analysis of organismal complexity in the multicellular green alga Volvox carteri. *Science* **329,** 223–226 (2010).
4. Rice, K. C. & Bayles, K. W. Molecular control of bacterial death and lysis. *Microbiol Mol Biol Rev* **72,** 85–109, table of contents (2008).
5. González-Pastor, J. E., Hobbs, E. C. & Losick, R. Cannibalism by Sporulating Bacteria. *Science* **301,** 510–513 (2003).
6. Claverys, J.-P., Martin, B. & Håvarstein, L. S. Competence-induced fratricide in streptococci. *Mol Microbiol* **64,** 1423–1433 (2007).
7. Riley, M. A. & Gordon, D. M. The ecological role of bacteriocins in bacterial competition. *Trends Microbiol* **7,** 129–133 (1999).
8. Perry, J. A., Cvitkovitch, D. G. & Lévesque, C. M. Cell death in Streptococcus mutans biofilms: a link between CSP and extracellular DNA. *FEMS Microbiol Lett* **299,** 261–266 (2009).
9. Ackermann, M. *et al.* Self-destructive cooperation mediated by phenotypic noise. *Nature* **454,** 987–990 (2008).
10. Tanji, Y., Asami, K., Xing, X.-H. & Unno, H. Controlled expression of lysis genes encoded in T4 phage for the gentle disruption of Escherichia coli cells. *Journal of Fermentation and Bioengineering* **85,** 74–78 (1998).
11. Pasotti, L., Zucca, S., Lupotto, M., Cusella De Angelis, M. G. & Magni, P. Characterization of a synthetic bacterial self-destruction device for programmed cell death and for recombinant proteins release. *J Biol Eng* **5,** 8 (2011).
12. Huh, J. H., Kittleson, J. T., Arkin, A. P. & Anderson, J. C. Modular design of a synthetic payload delivery device. *ACS Synth Biol* **2,** 418–424 (2013).
13. Wang, H. H. *et al.* Programming cells by multiplex genome engineering and accelerated evolution. *Nature* **460,** 894–898 (2009).
14. Kachroo, A. H., Kancherla, A. K., Singh, N. S., Varshney, U. & Mahadevan, S. Mutations that alter the regulation of the chb operon of Escherichia coli allow utilization of cellobiose. *Mol Microbiol* **66,** 1382–1395 (2007).
15. Gardner, T. S., Cantor, C. R. & Collins, J. J. Construction of a genetic toggle switch in Escherichia coli. *Nature* **403,** 339–342 (2000).
16. Ellis, T., Wang, X. & Collins, J. J. Diversity-based, model-guided construction of synthetic gene networks with predicted functions. *Nat Biotech* **27,** 465–471 (2009).
17. Egbert, R. G. & Klavins, E. Fine-tuning gene networks using simple sequence repeats. *Proc Natl Acad Sci USA* **109,** 16817–16822 (2012).
18. Cascales, E. *et al.* Colicin Biology. *Microbiol Mol Biol Rev* **71,** 158–229 (2007).
19. Bokinsky, G. *et al.* Synthesis of three advanced biofuels from ionic liquid-pretreated switchgrass using engineered Escherichia coli. *Proc Natl Acad Sci USA* **108,** 19949–19954 (2011).
20. Zhang, X.-Z., Sathitsuksanoh, N., Zhu, Z. & Percival Zhang, Y.-H. One-step production of lactate from cellulose as the sole carbon source without any other organic nutrient by recombinant cellulolytic Bacillus subtilis. *Metab Eng* **13,** 364–372 (2011).
21. Zhang, X.-Z., Sathitsuksanoh, N. & Zhang, Y.-H. P. Glycoside hydrolase family 9 processive endoglucanase from Clostridium phytofermentans: heterologous expression, characterization, and synergy with family 48 cellobiohydrolase. *Bioresour Technol* **101,** 5534–5538 (2010).

22. Liao, H., Zhang, X.-Z., Rollin, J. A. & Zhang, Y.-H. P. A minimal set of bacterial cellulases for consolidated bioprocessing of lignocellulose. *Biotechnol J* **6,** 1409–1418 (2011).
23. Farabaugh, P. J., Schmeissner, U., Hofer, M. & Miller, J. H. Genetic studies of the lac repressor. VII. On the molecular nature of spontaneous hotspots in the lacI gene of Escherichia coli. *J Mol Biol* **126,** 847–857 (1978).
24. Ghosal, D., Sommer, H. & Saedler, H. Nucleotide sequence of the transposable DNA-element IS2. *Nucleic Acids Res* **6,** 1111–1122 (1979).
25. Johnsrud, L. DNA sequence of the transposable element IS1. *Mol. Gen. Genet.* **169,** 213–218 (1979).
26. Hardin, G. The Tragedy of the Commons. *Science* **162,** 1243–1248 (1968).
27. Kerr, B., Neuhauser, C., Bohannan, B. J. M. & Dean, A. M. Local migration promotes competitive restraint in a host–pathogen 'tragedy of the commons'. *Nature* **442,** 75–78 (2006).
28. Sousa, A., Bourgard, C., Wahl, L. M. & Gordo, I. Rates of transposition in Escherichia coli. *Biology Letters* **9,** 20130838–20130838 (2013).
29. Csörgo, B., Fehér, T., Tímár, E., Blattner, F. R. & Pósfai, G. Low-mutation-rate, reduced-genome Escherichia coli: an improved host for faithful maintenance of engineered genetic constructs. *Microb Cell Fact* **11,** 11 (2012).
30. Tyo, K. E. J., Ajikumar, P. K. & Stephanopoulos, G. Stabilized gene duplication enables long-term selection-free heterologous pathway expression. *Nat Biotech* **27,** 760–765 (2009).
31. Babson, D. M., Held, M. & Schmidt Dannert, C. *Designer Microbial Ecosystems – Toward Biosynthesis with Engineered Microbial Consortia*. *Natural Products* 23–38 (John Wiley & Sons, Inc., 2014). doi:10.1002/9781118794623.ch2
32. Esvelt, K. M., Carlson, J. C. & Liu, D. R. A system for the continuous directed evolution of biomolecules. *Nature* **472,** 499–503 (2011).
33. Brenner, K., You, L. & Arnold, F. H. Engineering microbial consortia: a new frontier in synthetic biology. *Trends Biotechnol* **26,** 483–489 (2008).
34. Bernstein, H. C. & Carlson, R. P. Microbial Consortia Engineering for Cellular Factories: in vitro to in silico systems. *Comput Struct Biotechnol J* **3,** e201210017 (2012).

Box 1

i.

$$\dot{C} = \frac{n}{k_C + n} v_C C - \frac{n}{k_\sigma + n} \sigma C \quad (1)$$

$$\dot{A} = \frac{n}{k_A + n} v_A A + \frac{n}{k_\sigma + n} \sigma C - \rho A \quad (2)$$

$$\dot{F} = -\omega \rho A F \quad (3)$$

$$\dot{n} = \omega \rho A F - \frac{n}{\gamma}\left(\frac{v_C}{k_C + n} C + \frac{v_A}{k_A + n} A\right) \quad (4)$$

ii.

$$\dot{C} = (v_C - \sigma) C \quad (5)$$

$$\dot{A} = v_A A + \sigma C \quad (6)$$

iii.

$$\dot{C} = (v_C - \sigma) C \quad (5)$$

$$\dot{A} = (v_A - \rho) A + \sigma C \quad (7)$$

iv.

$$\dot{F} = -\omega \rho A F \quad (3)$$

$$Y(n) = \gamma n + b \quad (8)$$

v.

$$\dot{C} = (v_C - \sigma - \chi_C) C \quad (9)$$

$$\dot{S} = v_C S + \chi_C C \quad (10)$$

$$\dot{A} = (v_A - \rho - \chi_A) A + \sigma C \quad (11)$$

$$\dot{P} = v_A P + \chi_A A \quad (12)$$

i. We constructed a population scale model composed of first order ordinary differential equations. The model contains four relevant species: consumers (C), altruists (A), cellulose (F, feedstock), and digestible nutrients (n) with corresponding units of colony forming units per mL for cells and grams per mL for molecules (1-4). Consumer and altruist cells grow in the presence of nutrients at rates v_C and v_A, respectively. Individual consumer cells differentiate to altruists at rate σ, and altruists lyse at rate ρ. Altruist payloads degrade feedstock to nutrients at rate ω, and nutrients yield biomass Y according to γ. Nutrient-dependent dynamics are controlled by half maximal rate constants for growth (k_C, k_A) and differentiation (k_σ). Autolysis is considered nutrient-independent. Additional model details are included in Supplementary Table 1 and Supplementary Note 1.

Experimental Parameter Measurements

The modularity of the synthetic SDAc developmental gene network allows experimental measurement of each parameter by systematic deconstruction of the full system. We constructed simplified sub-models to identify the key circuit parameters and measured the behaviors of defined sub-circuits to estimate the parameters. Experimental details are described in the Materials and Methods and modeling approaches to the parameter estimates are described in detail in the Supplementary Information.

ii. Module I, differentiation rate (σ)
A continuous growth model of consumer and pseudo-altruists was used to estimate differentiation rate for payload and lysis deficient SDAc strains. The temporal population fraction of consumers (RFP producers) and altruists (GFP producers) was measured by flow cytometry for strains pre-induced to the consumer state, washed and grown in cellobiose (Figure 2a). For each strain σ estimates were fit to equations (5, 6) using growth rates measured independently.

iii. Module II, autolysis rate (ρ)
A continuous growth model of consumers and functional altruists was used to estimate autolysis rate for SDAc strains. Strains were initialized and measured as in Module I. For each strain ρ estimates were fit to equations (5, 7; Figure 2b) using growth rates and differentiation rates measured independently.

iv. Module III, cellulose hydrolysis (ω)
A model of feedstock degradation and nutrient release was used to estimate cellulose hydrolysis rates for lysis deficient SDAc strains expressing cellulase payloads. Crude cell lysates were generated from cellulase producing strains. Nutrient release from PASC media inoculated with cell lysates was measured via growth of a cellulase and lysis deficient strain. For each strain ω estimates were fit to equation (3) using nutrient estimates derived by applying equation (8) to growth data.

v. Cheater dynamics
A continuous growth model of consumers, altruists, consumer cheaters that do not differentiate (S) and altruist cheaters that do not lyse (P) was used to estimate rates of escape from consumer (χ_C) and altruist (χ_A) states. Models that account for individual or both cheater sub-populations were used as fits to the population fraction data obtained for Module II (9-12, Figure 4d).

Figures

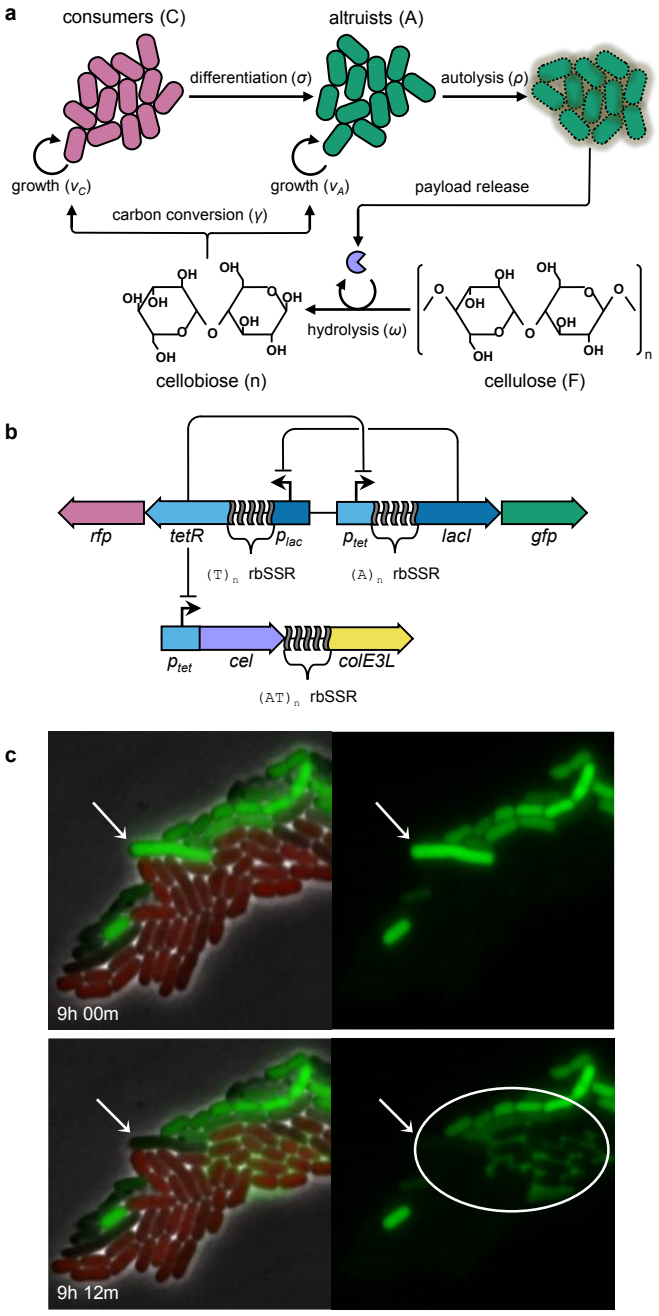

Figure 1. A synthetic developmental program for cooperative cellulose digestion. **(a)** Cellobiose consumers stochastically transition to self-destructive altruists. Altruists, in turn, produce and release cellulase payloads via autolysis to support the consumer population. **(b)** The genetic implementation of the SDAc developmental program includes a differentiation control plasmid (above) and a payload delivery plasmid (below). Cell states are mediated by a mutual inhibition toggle switch using transcriptional repressors LacI and TetR. TetR-dominant cells express RFP as consumers; LacI-dominant cells co-express cellulase and colE3 lysis (*colE3L*) proteins with GFP as altruists. Differentiation and lysis rates are fine-tuned with rbSSR sequences for *tetR* and *lacI* (differentiation) and *colE3L* (lysis). **(c)** Demonstration of differentiation and autolysis within a microcolony seeded by a single cell. A large altruist cell (white arrow) maintains its payload (upper panel) until it undergoes autolysis (lower panel), enabling GFP payload diffusion to surrounding cells (circle). See Supplementary Movie.

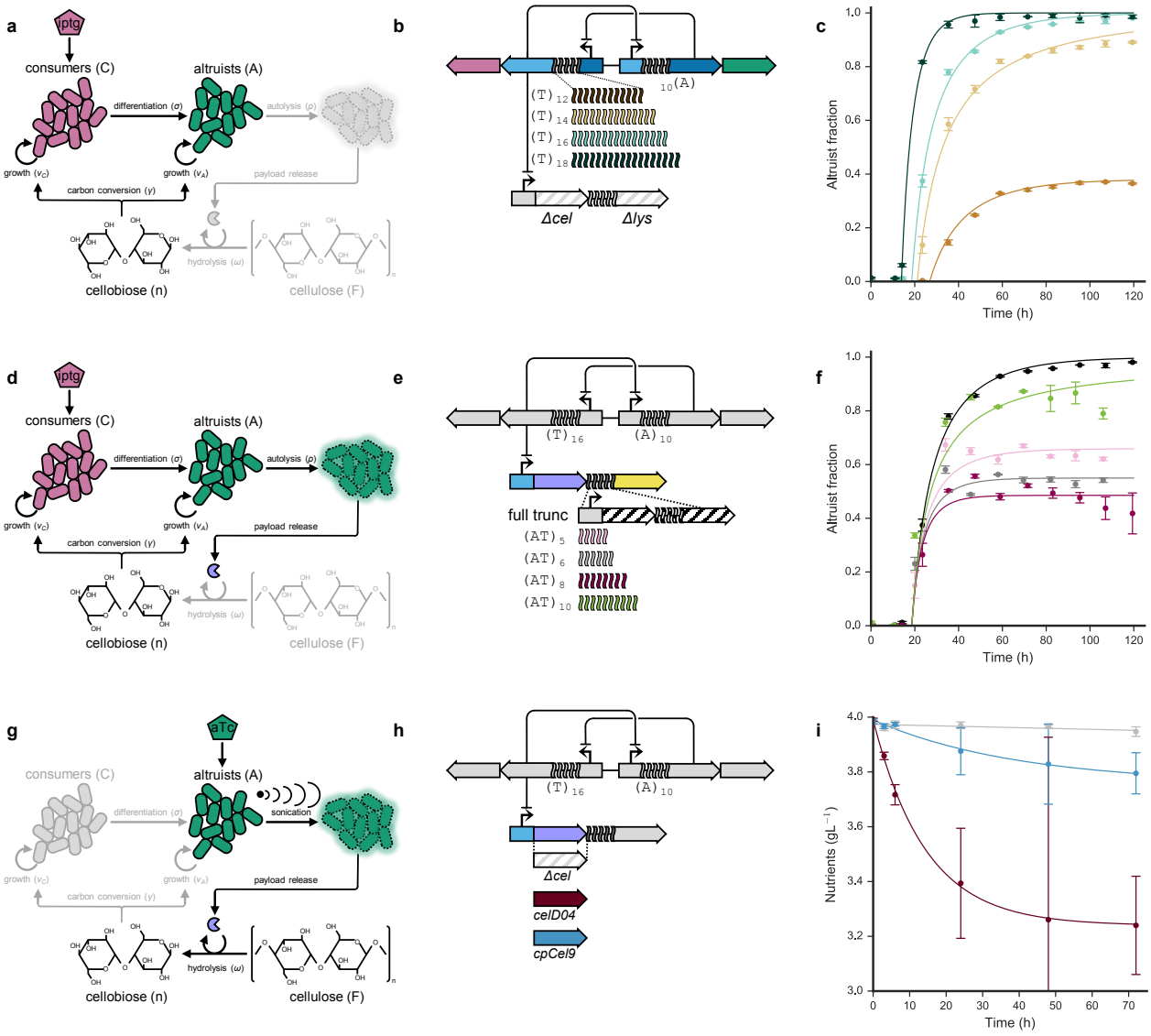

Figure 2. Parameter sweeps for differentiation, autolysis and cellulase activity. (a) For the differentiation assay, cultures were initialized to the consumer state using IPTG and grown continuously in cellobiose to differentiate into altruists deficient in cellulase and lysis. (b) Genetic variants tested for differentiation vary rbSSR repeat length to modulate TetR expression. Cellulase and lysis genes are removed from the payload plasmid. (c) Differentiation data and model fits to estimate σ (see Supplementary Note 4). (d) For the lysis assay, cultures were initialized as in (a) for consumers to differentiate into lysis-competent altruists. (e) Genetic variants tested for lysis used intermediate differentiator $(T)_{16}$, varying (AT)-rbSSR repeats driving lysis gene expression or using a control plasmid with no cellulase or lysis genes (ctl). (f) Lysis data and model fits to estimate ρ (see Supplementary Note 5). (g) For the cellulase activity assay, lysis-deficient strains were induced to the altruist state using aTc, growth to saturation and sonicated to generate crude cell extracts. (h) Genetic variants tests for cellulase activity by expressing different cellulases or maintaining a control plasmid (*Δcel*). (i) Cellulase activity data and model fits to estimate ω (see Supplementary Note 7).

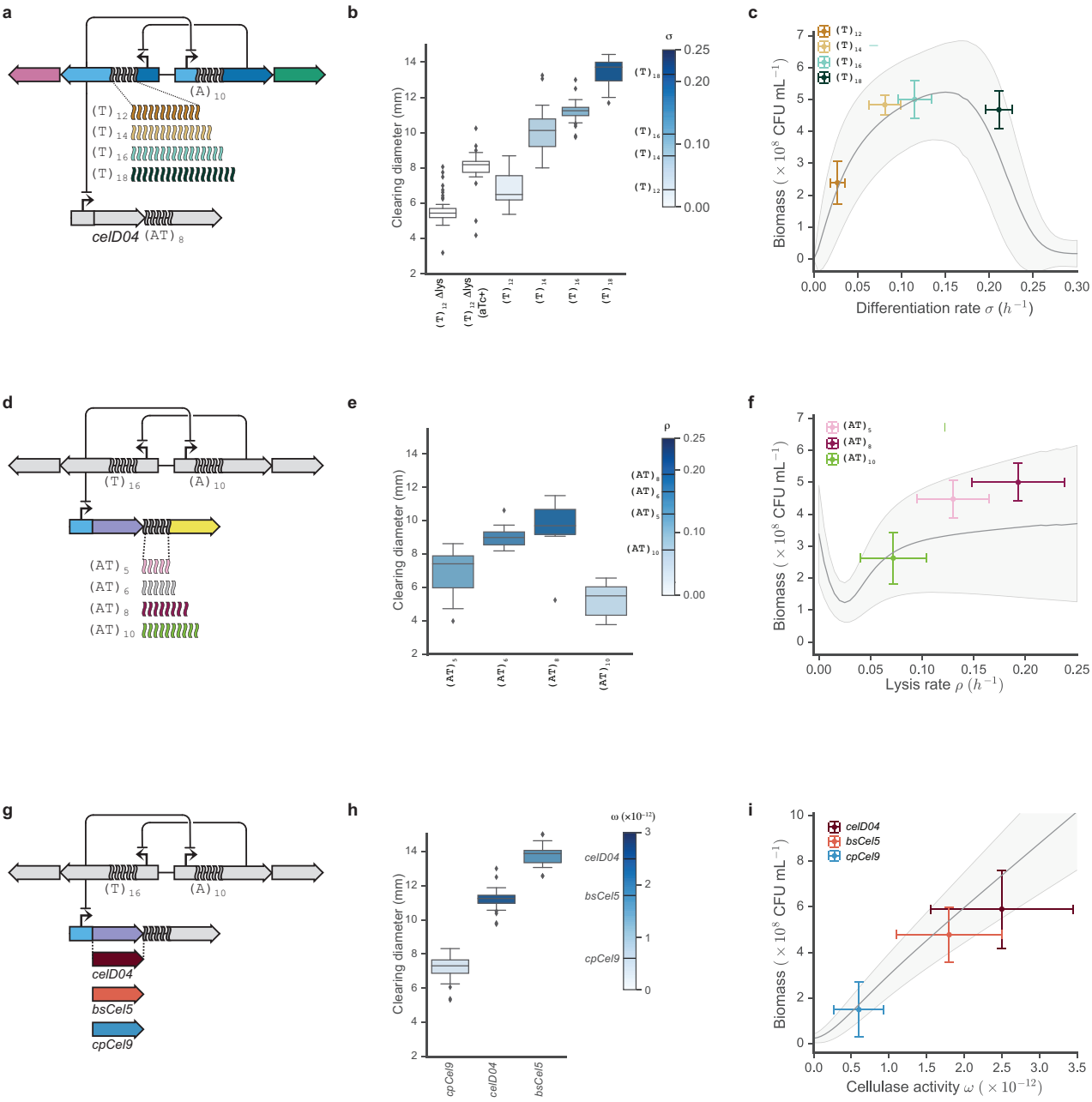

Figure 3. Characterization of cellulose hydrolysis and nutrient utilization reveals SDAc model prediction accuracy. (a) Differentiation rate variants expressing cellulase CelD04 with lysis rbSSR $(AT)_8$. (b) Clearing size distributions for individual colonies from differentiation variants in (a) (N = 31, 21, 17, 15, 6). (c) Growth titer in M9 minimal 0.4% PASC media after 72 hours for differentiation variants in (a). X-axis error bars represent standard deviation of the parameter estimate and y-axis error bars represent standard error for CFU counts from at least four replicates. One standard deviation of model uncertainty for cell growth is displayed as the shaded region. (d) Lysis rate variants for intermediate differentiator $(T)_{16}$ expressing cellulase CelD04. (e) Clearing size distributions for individual colonies from lysis variants in (d) (N = 20, 14, 11, 15). (f) Growth titer as in (c) for some lysis variants in (d). (g) Cellulase variants for intermediate differentiator $(T)_{16}$ and an optimal lysis rbSSR for each cellulase. (h) Clearing size distributions for individual colonies from cellulase variants in (g) (N = 20, 15, 16). (i) Growth titer as in (c) for cellulase variants in (g). Error bars for x-axis represent the interquartile range for each ω estimate. Whiskers shown for each box plot extend one interquartile range.

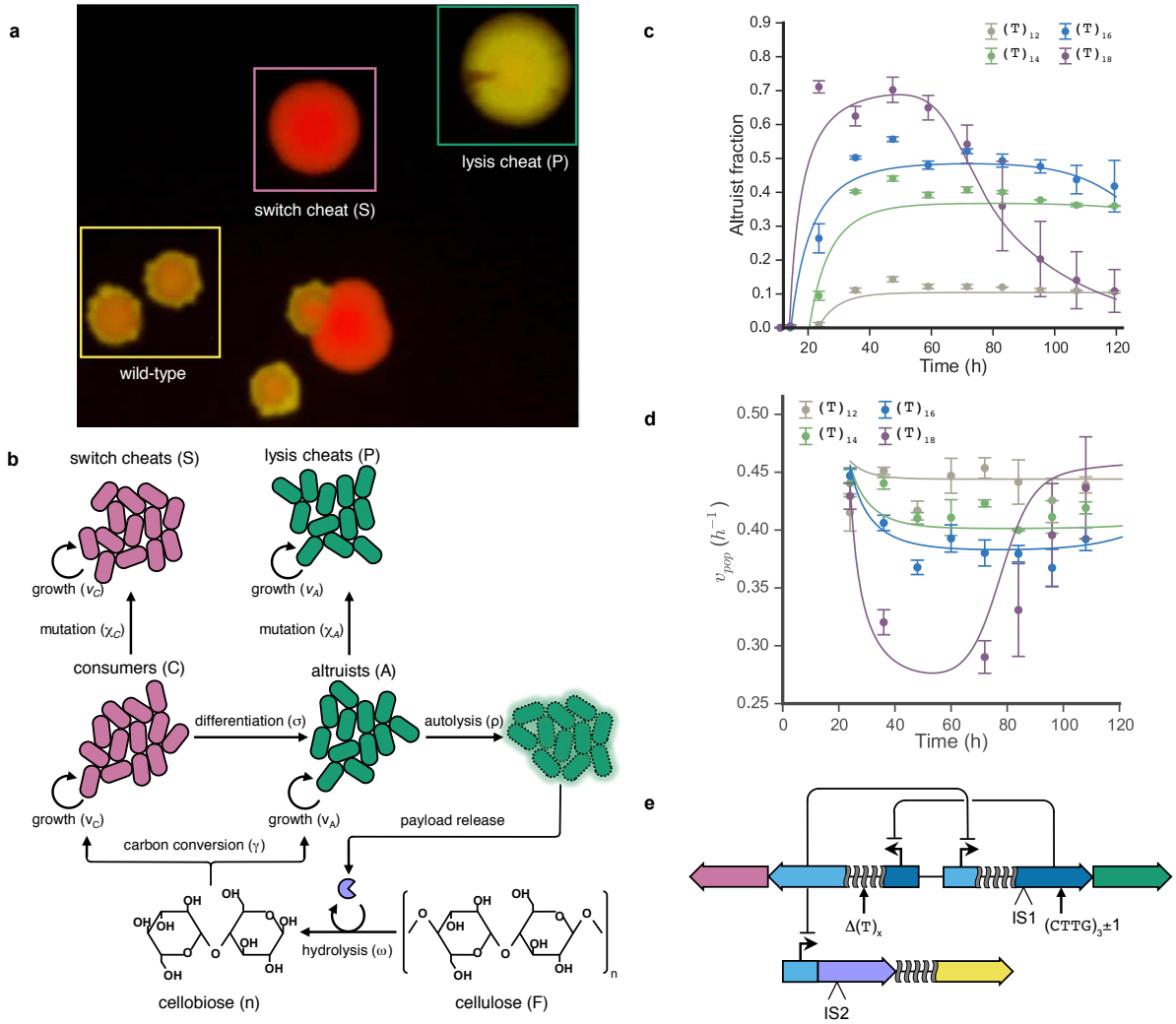

Figure 4 Mechanisms and rates of escape for SDAc cheaters. (a) Fluorescence image of wild-type and cheater colonies isolated from PASC cultures of hyperdifferentiator $(T)_{18}$ that no longer differentiate (S) or no longer lyse (P). (b) Representation of alternate SDAc model that incorporates mutational dynamics by including sink states for switch cheaters (S) and pseudo-altruist cheaters (P) with associated mutagenesis rates (see Box 1, module iv). (c) Dual cheater model fit to altruist fraction measurements for differentiation (compare to Supplementary Figure 5). Escape rate estimates for hyperdifferentiator $(T)_{18}$ are used for all altruist fraction fits. (d) Continuous growth model fit for bulk population growth rate v_{pop} measurements of differentiation variants, incorporating dual cheater rates from hyperdifferentiator $(T)_{18}$. (e) Summary of observed mutations that produce switch or pseudo-altruist cheaters. Switch mutants included an expansion or contraction of a native simple sequence repeat element in the *lacI* coding sequence, repeat unit truncations of rbSSR $(T)_{18}$ that controls differentiation rate and insertion sequence disruption of LacI expression. Insertion sequence disruption of the CelD04 gene (green arrows) were observed for altruist cheaters. For additional details on observed mutations see Supplementary Tables 10 and 11.

Materials and methods

Media

Rich media was prepared as LB Miller broth (Cat #244620, Difco), supplemented with 15 g L^{-1} bacto agar (Cat# 214030, Difco) when making solid media and with bacto agar and 0.1% carboxymethylcellulose (C5678, Sigma) to quantify cellulase clearings. M9 minimal media was prepared with M9 salts (Cat# 248510, Difco), 1 mM $MgSO_4$, 100 μM $CaCl_2$, supplemented with 1 mg mL^{-1} biotin and a carbon source (glucose, cellobiose or PASC) at concentrations specified in the text. M9 minimal 0.4% cellobiose plates for isolating cellobiose utilizer strains were prepared as above supplemented with 15 g L^{-1} bacto agar. Ampicillin and kanamycin antibiotics were supplemented when required at 20 μg mL^{-1} and 20 μg mL^{-1}, respectively, unless indicated.

PASC preparation

Phosphoric acid swollen cellulose (PASC) was prepared following a reported protocol[1]. Briefly, a cellulose slurry was created from sterile water and cellulose powder (Sigmacell 20, Sigma), combined with ice-cold 85% phosphoric acid (Sigma) and incubated at 4°C for 2 hours. Cellulose was precipitated in sterile water and washed repeatedly to remove the acid and bring the slurry to neutral pH.

Strains and plasmid construction

All strains used for assays in this study were derived from a variant of EcNR1[2] with genomic deletions of the *fim* operon, *ampR* and *lacIZ* (CT009). Cellobiose utilizer DL069 was used as parent strain for all SDAc variants. Control strains for cellobiose utilization were derived from progenitor strain CT009. All strains are listed in Supplementary Table 2.

Plasmid construction was carried out using standard Gibson assembly protocols (Gibson et al. 2009). PCRs were performed using Phusion PCR Master Mix (NEB, M0531L) with a T-100 thermal cycler (Bio-Rad). Synthetic oligonucleotides for cloning were synthesized by Integrated DNA Technologies. Gibson assemblies were transformed into cloning strain DH5alpha. Transformations were performed by electroporation at 1250 V using an Eppendorf 2510 electroporator. Transformants were cultured on LB Miller agar plates with appropriate antibiotic or LB liquid media (Difco) at 37°C. Plasmids were extracted using the QIAprep Spin Miniprep Kit. Plasmids were sequenced by Genewiz (Seattle, WA). All plasmid assemblies were performed with vector pSC101 vector pGA4A5 or p15A vector pGA3K3 [3].

Cellulase genes were synthesized following standard polymerase cycling assembly (PCA) protocols[4] using synthetic oligonucleotides provided by OligoCo, Inc. PCA was performed with Phusion polymerase and cloned into plasmids for sequence verification using Gibson Assembly.

Genome engineering

Cellobiose utilizer strain RGE531 was engineered using multiple cycles of multiplex genome engineering following Wang *et al.*[2]. *E. coli* strain CT009 was grown in LB Miller broth to OD 0.4-0.6 at 30°C, then heat shocked in a water bath for 15 minutes at 42°C. The culture was chilled via ice slurry and centrifuged for 3 minutes at 5000 rpm in a centrifuge (Legend XR1, Thermo Scientific) pre-chilled to 4°C. The supernatant was decanted and cells were resuspended in 3 mL of ice-cold sterile water. The resuspension was centrifuged again for 3 minutes at 5000 rpm and the supernatant decanted. The cell pellet was resuspended in 800 μL of ice-cold sterile water and transferred to a 1.5 mL microcentrifuge tube. Cells were centrifuged at 4000 x g for 1 minute (Accuspin Micro 17R, Fisher Scientific) pre-chilled to 4°C. Supernatants were aspirated by pipette and cell pellets were resuspended in 40 mL ice-cold sterile water.

Competent cells were transformed with an oligonucleotide cocktail targeting ribosome binding site variation of *chbB/A/C/F/G* or deletion of *chbR* (synthesized by OligoCo, Inc., see Supplementary Table 10) by electroporation at 1800V using an Eppendorf electroporator 2510. Transformants were recovered in 10 mL of M9 0.4% cellobiose media in a shaker flask and grown for 48-72 hours at 30°C with shaking. This process was repeated for two additional cycles, using the saturated recovery culture from the previous as the inoculum for the next cycle of mutagenesis. Following each outgrowth in cellobiose, individual colonies were screened for rapid growth on M9 0.4% cellobiose agar plates, and several variants were isolated for *chb* operon sequencing and further use.

Microscopy

Fluorescence microscopy of SDAc microcolonies was carried out using equipment and procedures described previously[3]. *E. coli* strain 2.320 was transformed with a differentiation plasmid (*tetR*/*lacI* switch with $(T)_{10}/(A)_{12}$ repeats, p15A origin) and a payload delivery plasmid (colicin E3 lysis gene with $(AC)_{11}$ repeat, colE1 origin). Individual colonies were grown to saturation in minimal M9CA media (M8010, Teknova), 50 µg mL^{-1} kanamycin and 20 µg mL^{-1} ampicillin. Cultures were diluted 100:1, grown for two hours with shaking at 32°C and vortexed to break up cell aggregates. 1 µL of the culture was added to a glass-bottomed microscopy dish (GWSB-3512, WillCo Wells BV) and cells were immobilized on the dish surface using a

nutrient agar slab prepared with M9CA media, as described above, and 1% bacto agar (Difco). Microscopy dishes were transferred to a Nikon Ti-S inverted microscope (Nikon Instruments) equipped with a Coolsnap-HQ camera (Roper Scientific) and an environmental chamber (In Vivo Scientific). Microcolony growth and fluorescent states were recorded every 15 min by capturing phase contrast, GFP and RFP images while the dishes were maintained at 32°C for 10 to 12 hours.

Measurements of growth, differentiation and lysis rates

Individual strains were initialized to the consumer state or altruist state (lysis-deficient control only) by inoculating individual colonies from a restreaked LB agar plate. The colonies were forced to the consumer state via IPTG induction (1 mM) or the altruist state via aTc induction (100 ng/mL) and grown at 37°C for 16 hours on LB agar media supplemented with ampicillin and kanamycin. Cultures were washed to remove inducer, inoculated 2000:1 into a well of a deep-well plate with 500 µL M9 minimal 0.4% cellobiose media supplemented with biotin and antibiotics as above, and grown at 37°C. To maintain exponential growth and low cell density, each culture was sampled every 12 hours and transferred to the cytometer (C6 with CSampler, Accuri) to measure culture density and the fluorescence distribution to determine the fraction of altruists. Growth rates between measurements were measured as a simple exponential fit using the initial cell density, the final cell density, and the number of hours between measurements. Each culture was diluted into fresh broth with a dilution factor defined by the culture density and the estimated growth rate. The dilution factors ranged from 5:1 to 50:1 every 12 hours. Growth rates and population fractions of consumers and altruists were calculated as described in Supplementary Notes 3 and 4, respectively.

Cell growth in PASC media

Cultures grown in PASC were initially inoculated into LB liquid culture with ampicillin and kanamycin from individual colonies restreaked on LB agar plates with the same antibiotics and IPTG to force the consumer state. Saturated cultures were transferred at 100:1 dilutions into M9 minimal PASC media and viable cell counts were periodically quantified by serial dilution and plating.

Measurements of carbon to biomass conversion efficiency

Carbon to biomass yield for cellobiose and PASC were measured using strains grown in M9 minimal media supplemented with increasing levels of each carbon source, up to 4 g L^{-1}. Cellobiose growth was quantified after 36 hours with cellulase and lysis deficient DL146 by serial dilution, plating and counting colonies. PASC growth was quantified after 72 hours with DL110 by the same method. All cultures were inoculated according to the PASC growth assay protocol and colony forming units were quantified for at least three replicates on

LB plates supplemented with ampicillin and kanamycin. The estimate for cellobiose was fit only to the linear, carbon-limited regime observed at concentrations less than 1g L^{-1} (see Supplementary Figure XX and Supplementary Note 6)

Measurements of cellulose degradation

Cellulase production strains for individual cellulases and cellulase cocktails were initialized by restreaking on LB agar plates supplemented with kanamycin (50 µg/mL), ampicillin (20 µg/mL) and aTc (100 ng/mL). Single colonies were transferred to 3 mL LB supplemented with kanamycin and ampicillin and grown to saturation overnight. Turbid 1 mL cultures were sonicated on ice (Ultrasonic Cell Disruptor, SharperTek) to release intracellular cellulase. The sonicator settings were 15 minutes with 95% power, and 75% duty cycle of 20 seconds on and 10 seconds off. Viable cell counts were measured before and after sonication using serial dilution and CFU plating to measure cell lysis efficiency (ρ). Cell lysates were filtered (0.4 micron filter, Company) to generate sterile supernatant. 10 µL cellulase lysate was transferred to 1 mL of 0.4% M9 minimal PASC + biotin media and incubated at 37°C for 72 hours, periodically measuring cellulose degradation by Congo Red absorbance or nutrient release. Uniprot identifiers for cellulases are Q45430 (CelD04), P10475 (BsCel5) and A9KT90 (CpCel9).

Congo Red absorbance measurements were taken by sampling 100 uL of the PASC growth media with cellulase at 0, 6, 12, 24, 48 and 72 hours post-inoculation, adding 100uL 0.15% (w/v) aqueous Congo red. After staining for 30 minutes, samples were centrifuged at 5000 rpm (Legend XR1) and 100 µL of PASC supernatant was transferred to a clear, flat-bottom microwell plate (Corning 2595). Absorbance readings were measured by plate reader (Biotek) at a wavelength of 480 nm.

Cellulolytic release of digestible nutrients was estimated by measuring DL146 growth on PASC supernatant after lysate incubation. 10 µL aliquots of sterile cell lysates, prepared as above, were inoculated in 1 mL M9 minimal 0.4% PASC media, prepared in parallel for each time measurement. At each time point, 1 mL PASC samples were centrifuged in triplicate to pellet the PASC and collect the supernatant. DL146 cultures were grown for 36 hours in the supernatant media and culture densities were measured by serial dilution and plating.

Congo Red clearing assay

Individual colonies were generated on LB agar containing cellulose and the plates were stained with Congo Red dye to observe clearings. Strains were incubated for 14 hours on LB Miller agar supplemented with

kanamycin, ampicillin and 0.1% carboxymethylcellulose. Colonies were removed from plates by washing with 70% ethanol. Plates were stained with 0.1% Congo Red for 20 minutes and destained with 1 M NaCl in two rinse steps, destaining for 5 minutes and 30 minutes, respectively. Clearing diameter for each colony was quantified from bright-field images of the stained plates by measuring clearing diameter using ImageJ software. Clearing diameter was converted from pixels to millimeters by normalizing to known plate diameter.

Sequencing SDAc switching or lysis cheaters

Bright, monochromatic red or green fluorescent colonies isolated from six replicate cultures of $(T)_{18}/(A)_{10}$ grown in M9 minimal 0.4% PASC media for 72 hours were identified via blue light transillumination. Each colony was replated separately on an LB agar plate and an LB agar plate supplemented with kanamycin and ampicillin to test for plasmid loss. Sequencing was performed on individual colonies by Genewiz, Inc. Differentiation plasmids were sequenced at the dual promoter region (BSSregSeq_2809) and the *lacI* C-terminal sequence (lacIrptSeq_2810). Payload plasmids were sequenced across the payload transcription unit (oligos Vf2 & Vr). Sequencing oligos are listed in Supplementary Table 13.

Materials and Methods References

1. Zhang, Y. H. P., Cui, J., Lynd, L. R. & Kuang, L. R. A transition from cellulose swelling to cellulose dissolution by o-phosphoric acid: evidence from enzymatic hydrolysis and supramolecular structure. *Biomacromolecules* **7,** 644–648 (2006).
2. Wang, H. H. *et al.* Programming cells by multiplex genome engineering and accelerated evolution. *Nature* **460,** 894–898 (2009).
3. Egbert, R. G. & Klavins, E. Fine-tuning gene networks using simple sequence repeats. *Proc Natl Acad Sci USA* **109,** 16817–16822 (2012).
4. Hoover, D. M. & Lubkowski, J. DNAWorks: an automated method for designing oligonucleotides for PCR-based gene synthesis. *Nucleic Acids Res* **30,** e43 (2002).

Supplementary Information

Self-destructive altruism in a synthetic developmental program enables complex feedstock utilization

Robert G. Egbert[1], Leandra M. Brettner[2], David Zong[2], Eric Klavins[1]

1. Electrical Engineering Department, University of Washington, Seattle, WA, USA
2. Bioengineering Department, University of Washington, Seattle, WA, USA

Table of Contents:

Supplementary Figure 1. Engineering cellobiose utilization for SDAc strains

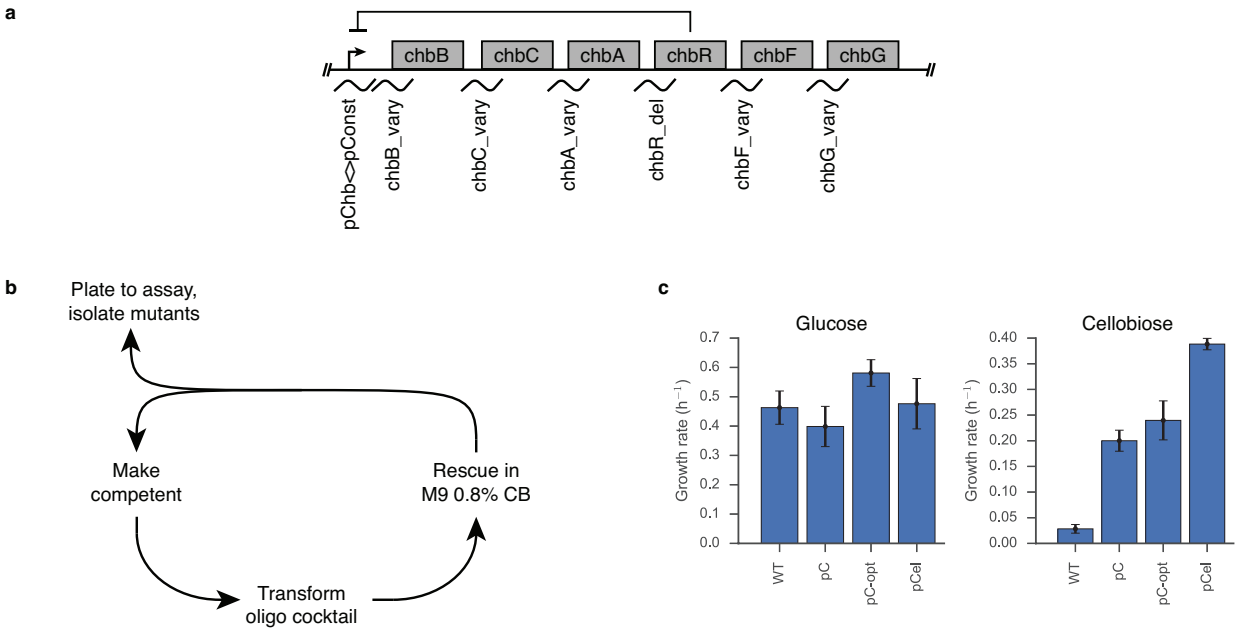

(a) Chitobiose (*chb*) operon with targeted sites for promoter replacement (pChb), overexpression (*chbA*, *chbB*, *chbC*, *chbF*, *chbG*) or deletion (*chbR*). See Supplementary Table 11 for oligonucleotide sequences. **(b)** Workflow to select for variants that grow faster on cellobiose. **(c)** Growth rates for a selection of variants: wild-type (WT, EcNR1 Δfim ΔlacIZ), the native *chb* promoter replaced with a constitutive promoter (pC, RGE531), the fastest growing recombinant mutant (pC-opt, DL069) and a control strain (pCel, DL180) that expresses a membrane-bound beta-glucosidase from *Cellvibrio japonicas*[1]. Growth rates were measured at 32°C in a Biotek Synergy plate reader (n=3) using 200 µL cultures grown in 96-well microwell plates.

Supplementary Figure 2. Parameter sweeps for cellulose utilization model

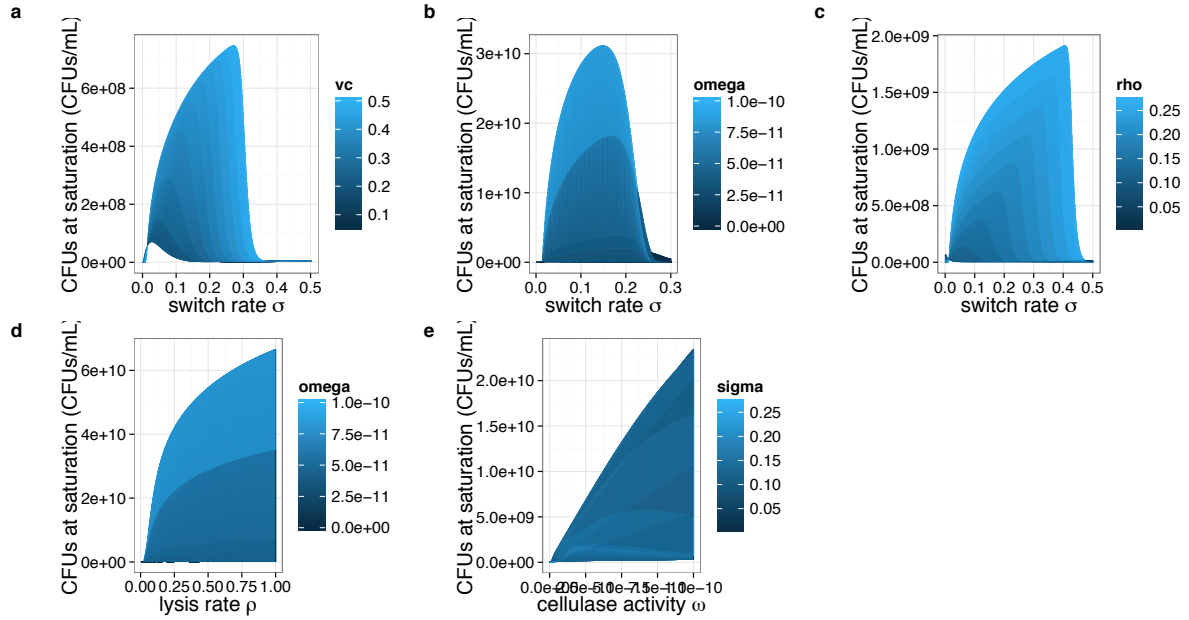

Parameter sweeps of core SDAc model parameters to develop intuition for circuit behavior and to guide system implementation. When plots do not vary parameters, nominal values are $v_c = v_a = 0.4$, $\sigma = 0.1$, $\rho = 0.25$, $\omega = 1.0\times10^{-11}$. **(a-c)** Expected biomass yield as a function of differentiation rate for discrete growth **(a)**, cellulase activity **(b)** and lysis **(c)** rates. **(d, e)** Expected biomass yield as a function of lysis rate for discrete cellulase activity rates **(d)** and as a function of cellulase activity rates for discrete differentiation rates **(e)**.

Supplementary Figure 3. Data collection for growth, differentiation and lysis rates

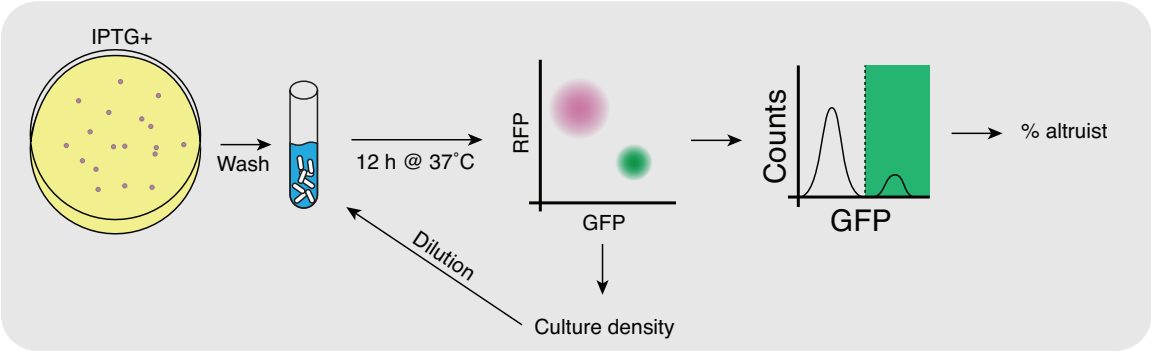

Experimental workflow to estimate growth, differentiation and lysis rates using low-density continuous culture and flow cytometry. Cultures are initialized in the consumer state by growing individual colonies on LB agar supplemented with IPTG. Colonies are washed and diluted into M9 minimal cellobiose media and periodically sampled in the flow cytometer to calculate the population fraction of differentiated cells and the dilution factor for the next growth passage.

Supplementary Figure 4. Mapping differentiation rate to differentiation delay

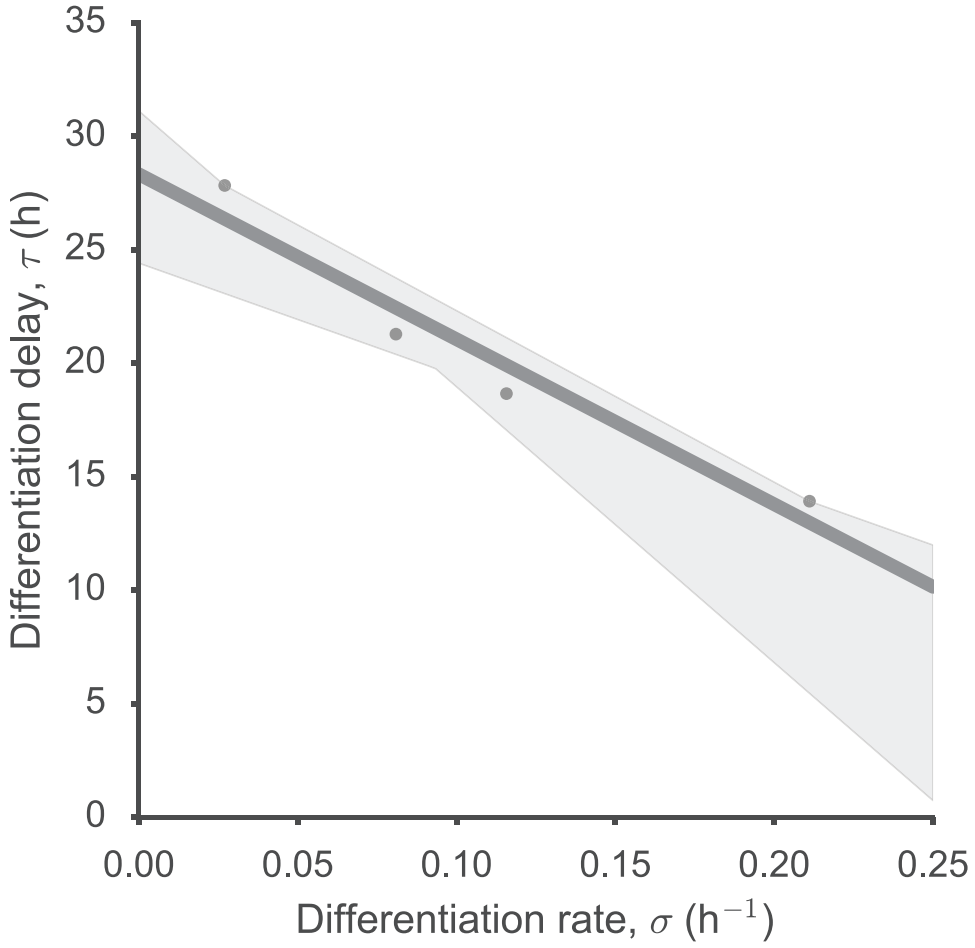

Relationship between the differentiation rate to the delay in the initiation of switching following the removal of IPTG inducer for strains DL046, DL112, DL110 and DL108. Linear fit line is $y = 28.3 - 72.7x\ h$. The shaded area represents a 95% confidence interval.

Supplementary Figure 5. Altruist fraction fits combining growth, differentiation and lysis parameters

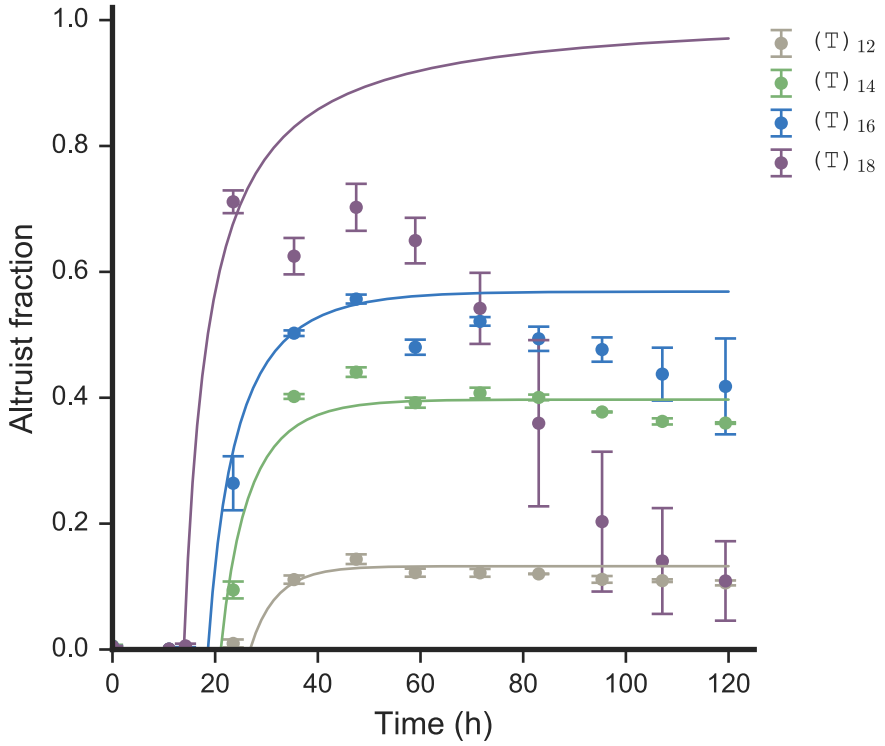

Altruist fractions were calculated from measurements of the continuous culture differentiation experiment (N=3). Curves are derived from model predictions using growth rates of DL147, differentiation rates for the appropriate switch variant and the lysis rate for DL112, utilizing $(AT)_8$ rbSSR for ColE3L expression. Data for labels $(T)_{12}$, $(T)_{14}$, $(T)_{16}$ and $(T)_{18}$ correspond to measurements for strains DL046, DL112, DL110 and DL108, respectively (n=3).

Supplementary Figure 6. Mapping *colE3L* `(AT)` rbSSR length to lysis rate

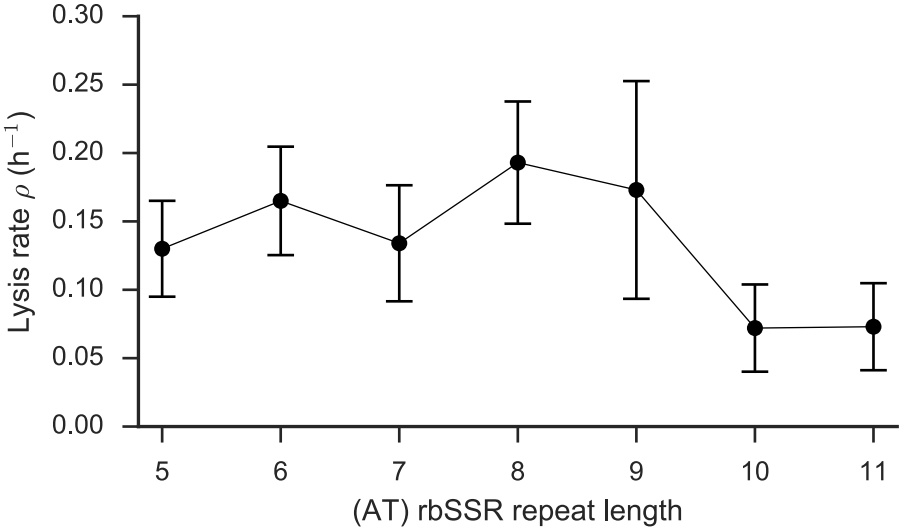

Lysis rate fits as a function of (AT) repeat length for multiple strains with switch $(T)_{16}$. Error bars represent parameter estimate uncertainty, inclusive of measurement error and parameter bootstrapping from growth rates and differentiation rates.

Supplementary Figure 7. Mapping cellulose degradation clearings to differentiation and lysis rates

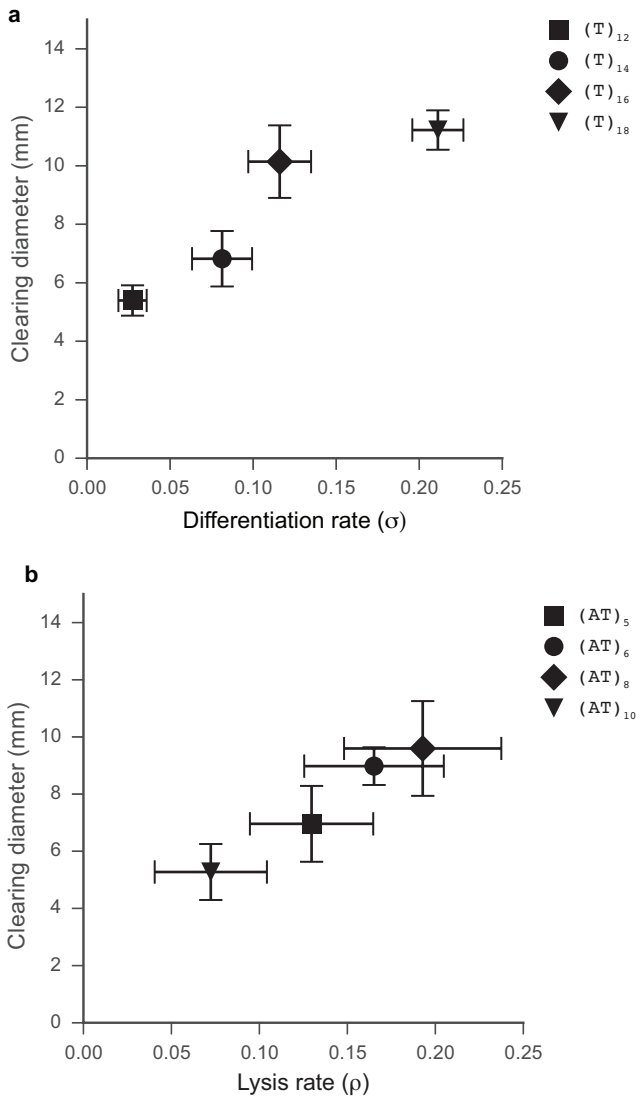

(a) Plot of cellulose degradation clearings as a function of differentiation rate for SDAc variants of the *tetR* rbSSR. (b) Plot of cellulose degradation clearings as a function of lysis rate for SDAc variants of the *colE3L* lysis gene rbSSR. For each panel the x-axis error bars represent uncertainty of experimental measurements and parameter bootstrapping and the y-axis error bars represent standard error from at least six replicate clearings of individual colonies (see Figure 3 caption).

Supplementary Figure 8. Carbon to biomass yield estimates

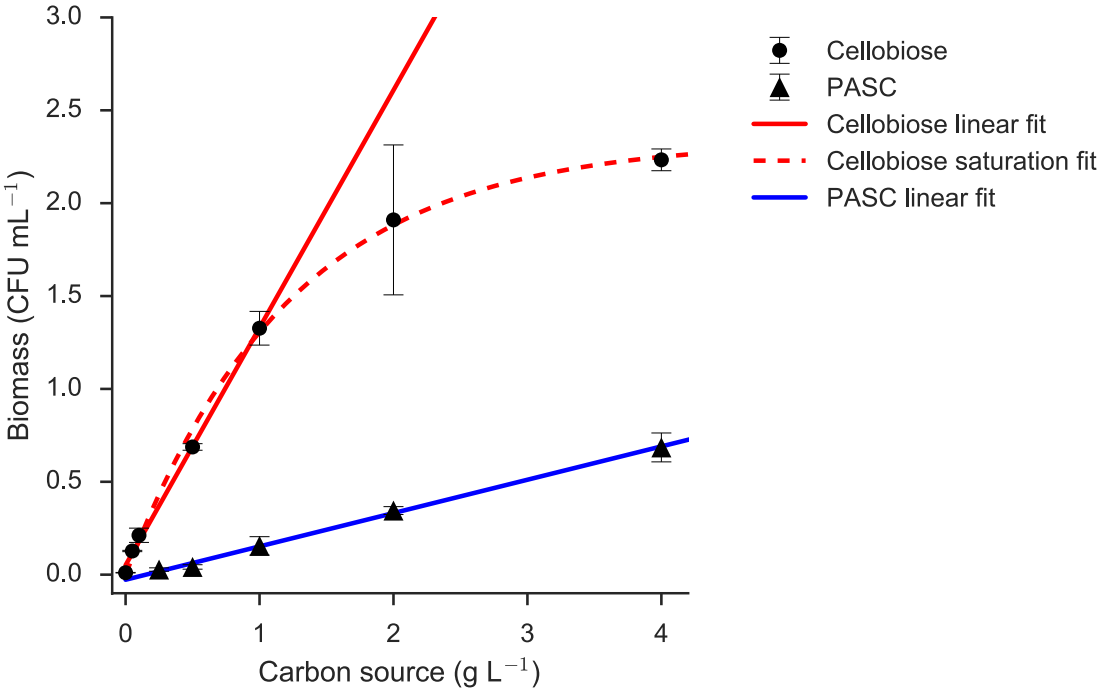

Carbon utilization measurements and fits for DL146 (cellobiose) and DL110 (PASC).

Supplementary Movie

Movie S1 shows the growth and differentiation dynamics of individual microcolonies derived from individual cells of the (T)10/(A)12 rbSSR-BSS switch variant with an inactive cellulase gene and colicin E3 lysis gene expression controlled by an $(AC)_{11}$ rbSSR, transformed in strain 2.320. The movie demonstrates the stochastic differentiation and delayed lysis dynamics underlying SDAc behavior. The movie scale bar is 5 μm.

Supplementary Table 1. SDAc model parameters

Parameter	Description	Units
v_C, v_A	Consumer, altruist growth rates	h^{-1}
k_C, k_A	Half maximal growth constants	g
σ	Differentiation rate	h^{-1}
k_σ	Half maximal differentiation constant	g
ρ	Lysis rate	h^{-1}
ω	Cellulase activity	CFU^{-1} mL
γ	Nutrient to biomass conversion efficiency	CFU g^{-1}

Supplementary Table 2. List of strains used

Strain ID	Switch variant*	Payload	colE3 lysis repeat	Parent strain	Modifications
CT009	N/A	N/A	N/A	EcNR1	Δ*fimAICDFGH* Δ*ampR* Δ*lacIZ*
RGE531	N/A	N/A	N/A	CT009	pChb<>pConst,
DL046	$(T)_{12}/(A)_{10}$	CelD04	$(AT)_8$	DL069	
DL069	N/A	N/A	N/A	CT009	pChb<>pConst, Δ*chbR*, Δ(λ-Red)
DL108	$(T)_{18}/(A)_{10}$	CelD04	$(AT)_8$	DL069	
DL110	$(T)_{16}/(A)_{10}$	CelD04	$(AT)_8$	DL069	
DL112	$(T)_{14}/(A)_{10}$	CelD04	$(AT)_8$	DL069	
DL146	$(T)_{12}/(A)_{10}$	None	No lysis gene	DL069	
DL147	$(T)_{12}/(A)_{10}$	CelD04	No lysis gene	DL069	
DL180	N/A	CelD04	No lysis gene	CT009	Δ(λ-Red), pCellulose[1] (ampR), mRFP1 (kanR)
DL182	$(T)_{16}/(A)_{10}$	None	No lysis gene	DL069	
DL183	$(T)_{14}/(A)_{10}$	None	No lysis gene	DL069	
DL188	$(T)_{18}/(A)_{10}$	None	No lysis gene	DL069	
DL202	$(T)_{16}/(A)_{10}$	BsCel5	$(AT)_7$	DL069	
DL261	$(T)_{16}/(A)_{10}$	CpCel9	$(AT)_7$	DL069	
DL268	$(T)_{16}/(A)_{10}$	CelD04	$(AT)_5$	DL069	
DL269	$(T)_{16}/(A)_{10}$	CelD04	$(AT)_6$	DL069	
DL270	$(T)_{16}/(A)_{10}$	CelD04	$(AT)_7$	DL069	
DL271	$(T)_{16}/(A)_{10}$	CelD04	$(AT)_9$	DL069	
DL272	$(T)_{16}/(A)_{10}$	CelD04	$(AT)_{10}$	DL069	
DL273	$(T)_{16}/(A)_{10}$	CelD04	$(AT)_{11}$	DL069	
DL292	$(T)_{12}/(A)_{10}$	CpCel9	No lysis gene	DL069	
DL294	$(T)_{12}/(A)_{10}$	BsCel5, CpCel9	No lysis gene	DL069	
DL296	$(T)_{12}/(A)_{10}$	CelD04, CpCel9	No lysis gene	DL069	
DL307	$(T)_{12}/(A)_{10}$	BsCel5	No lysis gene	DL069	
DL322	$(T)_{16}/(A)_{10}$	BsCel5, CpCel9	$(AT)_9$	DL069	
DL329	$(T)_{12}/(A)_{12}$	CelD04	colE3	DL069	
DL327	$(T)_{16}/(A)_{10}$	CelD04, CpCel9	$(AT)_9$	DL069	

* $(T)_x/(A)_y$ indicates *x* poly-T rbSSR repeats driving TetR expression and *y* poly-A repeats driving LacI expression for the differentiation plasmid.

Supplementary Table 3. Cellobiose growth rates for SDAc strains

Strain ID	Switch variant	Cellulase	Lysis	Induction state*	Growth rate (hr^{-1})	StD
DL146	$(T)_{12}/(A)_{10}$	None	None	Consumer	0.463	0.01
DL146	$(T)_{12}/(A)_{10}$	None	None	Altruist	0.391	0.01
DL147	$(T)_{12}/(A)_{10}$	CelD04	None	Consumer	0.459	0.00
DL147	$(T)_{12}/(A)_{10}$	CelD04	None	Altruist	0.413	0.02
DL046	$(T)_{12}/(A)_{10}$	CelD04	colE3	Consumer	0.438	0.01
DL112	$(T)_{14}/(A)_{10}$	CelD04	colE3	Consumer	0.420	0.01
DL183	$(T)_{14}/(A)_{10}$	None	None	Consumer	0.430	0.01
DL110	$(T)_{16}/(A)_{10}$	CelD04	colE3	Consumer	0.389	0.01
DL182	$(T)_{16}/(A)_{10}$	None	None	Consumer	0.423	0.01
DL108	$(T)_{18}/(A)_{10}$	CelD04	colE3	Consumer	0.266	0.04
DL188	$(T)_{18}/(A)_{10}$	None	None	Consumer	0.395	0.00

* Induction to consumer state implies IPTG induction (1 mM). Induction to altruist state implies aTc induction (100 ng/mL).

Supplementary Table 4. Differentiation rates for lysis-deficient SDAc switch variants

Strain ID	Switch variant	σ (h^{-1})	StDev	τ (h)	StDev
DL146	$(T)_{12}/(A)_{10}$	0.027	0.009	26.8	4.56
DL183	$(T)_{14}/(A)_{10}$	0.081	0.018	21.1	0.97
DL182	$(T)_{16}/(A)_{10}$	0.116	0.019	18.6	0.78
DL188	$(T)_{18}/(A)_{10}$	0.211	0.015	13.9	0.03

Supplementary Table 5. Lysis rates for SDAc switch and lysis variants

Strain ID	Switch variant	Lysis variant	σ (h^{-1})	ρ (h^{-1})	StDev
DL046	$(T)_{12}/(A)_{10}$	$(AT)_8$	0.027	0.180	0.080
DL112	$(T)_{14}/(A)_{10}$	$(AT)_8$	0.081	0.159	0.052
DL108	$(T)_{18}/(A)_{10}$	$(AT)_8$	0.211	0.430	0.050
DL268	$(T)_{16}/(A)_{10}$	$(AT)_5$	0.116	0.130	0.035
DL269	$(T)_{16}/(A)_{10}$	$(AT)_6$	0.116	0.165	0.040
DL270	$(T)_{16}/(A)_{10}$	$(AT)_7$	0.116	0.134	0.042
DL110	$(T)_{16}/(A)_{10}$	$(AT)_8$	0.116	0.192	0.048
DL271	$(T)_{16}/(A)_{10}$	$(AT)_9$	0.116	0.173	0.080
DL272	$(T)_{16}/(A)_{10}$	$(AT)_{10}$	0.116	0.072	0.032
DL273	$(T)_{16}/(A)_{10}$	$(AT)_{11}$	0.116	0.073	0.032

Supplementary Table 6. Carbon to biomass yields for cellobiose and PASC

Media	Linear range	γ (CFU g^{-1})	StDev	R^2
Cellobiose	0 – 1 g L^{-1}	1.279e+12	3.344e+10	0.9919
PASC	0 – 4 g L^{-1}	1.795e+11	8.475e+09	0.9825

Supplementary Table 7. Cellulase activity measurements for cellulase production strains

Strain ID	Cellulase	ω (hydrolysis)	StDev	ω (biomass)	StDev
DL292	CpCel9	4.6e-12	2.4e-13	3.6e-13	3.9e-13
DL147	CelD04	5.7e-12	6.8e-13	1.6e-12	5.3e-13
DL294	CelD04 + CpCel9	6.8e-12	9.5e-13	1.8e-12	5.6e-13
DL307	BsCel5	6.1e-12	9.8e-13	1.2e-12	2.9e-13
DL294	BsCel5 + CpCel9	7.4e-12	4.3e-13	1.9e-12	3.0e-13

Note: units for ω are CFU^{-1} mL

Supplementary Table 8. Half-maximal rate constants for growth and differentiation

Parameter	Fit	StDev
k_C, k_A	0.00112	0.00045
k_σ	0.09999	0.00019

Supplementary Table 9. Cheater rates for expanded SDAc model

Cheater type(s)	χ_C (h^{-1})	StDev	χ_A (h^{-1})	StDev
Differentiation	2.688e-06	2.399e-06	n/a	n/a
Differentiation and lysis	1.177e-05	9.953e-06	7.368e-05	3.565e-05

Supplementary Table 10. Genotypes for differentiation cheaters

Plate Replicate	Isolation condition	Promoter mutation	*lacI* mutation
2	LB	None	None
2	LB kan/amp	None	$(CTGG)_2$
2	LB kan/amp	None	None
3	LB kan/amp	None	IS2 insertion at base 15 of *lacI*
3	LB kan/amp	None	IS2 insertion at base 15 of *lacI*
3	LB kan/amp	None	IS2 insertion at base 34 of *lacI*
4	LB	None	$(CTTG)_4$
4	LB	None	148 bp *lacI* deletion (A351)
4	LB kan/amp	None	None
4	LB kan/amp	None	$(CTTG)_4$
5	LB kan/amp	None	$(CTTG)_4$
5	LB kan/amp	None	$(CTGG)_2$
5	LB kan/amp	None	$(CTTG)_4$
5	LB kan/amp	None	20 bp *lacI* deletion (A303)
6	LB kan/amp	$\Delta(T)_5$	None
6	LB kan/amp	None	$(CTGG)_2$
6	LB kan/amp	$\Delta(T)_5$	None
6	LB kan/amp	$\Delta(T)_5$	None

Sequencing results of differentiation plasmid mutations from monochromatic RFP-positive $(T)_{18}/(A)_{10}$ escape colonies (six replicate plates). The first replicate plate had no mutations at the sequenced loci for the differentiation plasmid.

Supplementary Table 11. Genotypes for lysis cheaters

Plate Replicate	Isolation condition	Payload plasmid mutations
1	LB	None
1	LB Kan/Amp	None
2	LB	None
2	LB	None
2	LB	None
2	LB Kan/Amp	None
2	LB Kan/Amp	None
2	LB Kan/Amp	None
2	LB Kan/Amp	None
3	LB	None
4	LB	IS1 insertion at A514 in celD04
4	LB	IS1 insertion at A514 in celD04
4	LB Kan/Amp	IS1 insertion at A514 in celD04
4	LB Kan/Amp	IS1 insertion at A514 in celD04
5	LB	None
6	LB	None
6	LB	None
6	LB Kan/Amp	None

Sequencing results of payload plasmid mutations from monochromatic GFP-positive $(T)_{18}/(A)_{10}$ escape colonies (six replicate plates).

Supplementary Table 12. Oligonucleotides used to modify *chb* operon and for sequencing cheater genotypes

Oligo name	Sequence
pChb<>pConst	CTTCCATGCTCTGGGTAACTTGCGAAACCAACATGATGAATCTATTATAAAAAAAAAAAAAAAAA AAGTCAATACTCTATCGAACTCAGGCCAAAAAAAACCGGCGCAATGGCCGGTTTC
chbR_del	ggacataaataatccagcaacaggacagatatgtgaattgtcaggtataacgacttactgcatcg actccttatgccttcagttttcatgaagctcaattaattcagtaatcagttcac
chbA_A15	agctcttcagcttccgtttgcgtatcgggaatgttatcgagatccatcatTTTTTTTTTTTTTTT CCTCCTCttttcttaccggcacgattacccgtaccggcatcgattaaaatttcag
chbC_T15	actgcaaaagggaggagtacctttcaagcgatgcaataacattactcatAAAAAAAAAAAAAAA CCTCCTaaaaaccgcaatttaaatattgcggtattgatttatgaaataactcttt
chbB_A15	gaggtagacatgcccgcagaacaaaacagataaatgtgtttcttttccatTTTTTTTTTTTTTTT ACCTCCTGATatcgacgattatctgtcagccagacactccgcaagccttaacctg
chbF_A5	gtatagctgctcccgccaccaatagtgacgacttttaatttctggctcatTTTTTACCTCCTagt acagaatactgatatctggcatatctgccccccggacataaata
chbF_A15	gtatagctgctcccgccaccaatagtgacgacttttaatttctggctcatTTTTTTTTTTTTTTT ACCTCCTagtacagaatactgatatctggcatatctgccccccggacataaata
chbG_T15	cctttgcttaagccaaaatcatcggcattaacaatcagtaagcgttccatAAAAAAAAAAAAAAA CCTCCttaatgtgctttttaagctctgcgatgcagtcggcaaagtttggcagcc
BSSregSeq_2809	GGCTGCTCTACACCTAGCTTCTGG
lacIrptSeq_2810	GGTTTGTTGAAAACCGGACATGG
Vf2	TGCCACCTGACGTCTAAGAA
Vr	ATTACCGCCTTTGAGTGAGC

Supplementary Note 1. Model assumptions for SDAc population dynamics

The model for synthetic self-destructive altruism dynamics relies on multiple assumptions to minimize the number of parameters. First, intracellular enzyme accumulation is considered independent of the lysis rate, resulting in a fixed payload size per altruist. Second, cellulase dynamics were removed from the system of equations based on an assumption that cellulase enzymatic activity occurs much faster than its degradation, allowing parameters to be consolidated. Cellulase activity ω is normalized to the altruist population through the product ρA. Third, while we assume nutrient-dependent rates for growth and switching, altruist commitment to lysis is considered to be nutrient independent.

Supplementary Note 2. Parameter bootstrapping for SDAc models

Bootstrapping based on Monte Carlo simulations was used to generate many parameter estimates for SDAc models. Uncertainty in the parameter estimates depend both on experimental measurement error and independently measured experimental parameters. Parameter estimates should reflect both the fit to the experimental data and uncertainty propagated from parameters used to constrain the fit. Thousands of parameter fits were generated to propagate the uncertainty measures, randomly sampling from a normal distribution of the existing parameters for each fit[2]. We calculated the mean and standard deviation of the ensemble of fits to generate the parameter estimate.

Supplementary Note 3. Estimating growth rates from cytometry data

As described in the methods section, the growth rates for consumer cells and altruist cells were estimated by applying an exponential fit to cell densities measured via cytometry at 12 hour intervals in periodically diluted samples. The growth rate for each strain over three passage intervals (36, 48, 60 h) was measured in triplicate to obtain mean and standard error measurements for each strain (Supplementary Table 2).

For each strain, growth rate α was estimated from time *t1* to time *t2* using equations

$$P_{t2} = P_{t1}\left(\frac{V_{tx}}{V_{tx}+V_w}\right)e^{\alpha(t2-t1)}, \tag{S1}$$

$$\alpha = \ln\left(\frac{P_{t2}}{P_{t1}}\left(\frac{V_{tx}+V_w}{V_{tx}}\right)\right)(t_2 - t_1)^{-1}, \tag{S2}$$

for which P_{t1} and P_{t2} are the cell densities measured in gated events per second at times *t1* and *t2*, respectively, V_{tx} is the transfer volume in µL between passages and V_w is the media volume in µL.

Supplementary Note 4. Estimating differentiation rates from cytometry data

As described in Box 1 and the methods section, the differentiation rate σ for individual strains was estimated by applying parameter bootstrapping for growth rate estimates to fit Equations (5-6) to the fraction of lysis-deficient altruists. Cytometry samples were processed using custom Matlab scripts as previously reported[3]. Briefly, samples were filtered using a fixed gate for forward scatter values between 16,000 and 100,000 and side scatter values between 10 and 7,000. The altruist subpopulation was determined by using a fixed threshold in the GFP channel (488 nm excitation with 533 nm bandpass emission filter) of 600, which captures less that 0.1% of the population for a non-fluorescent strain.

An analytical solution to consumer and lysis-deficient altruist populations that accounts for a temporal delay observed in differentiation experiments was generated from Equations (5-6) of Box 1:

$$C(t) = e^{(v_C-\sigma)(t-\tau)}, \quad \text{(S3)}$$

$$A(t) = \frac{\sigma\left(e^{v_A(t-\tau)} - e^{(v_C-\sigma)(t-\tau)}\right)}{v_A - v_C + \sigma}. \quad \text{(S4)}$$

Differentiation rate σ and corresponding delay τ were estimated from measurements of $\frac{A(t)}{A(t)+C(t)}$ fit to Equations (S3, S4) for the cellulase and lysis deficient SDAc strains shown in Figure 2c (see Supplementary Table 3 for values). Fits were generated using the Levenberg-Marquardt nonlinear least squares algorithm (nlsLM) in R. Differentiation delay was observed to be inversely proportional to the differentiation rate (see Supplementary Figure 4). Parameter bootstrapping was performed to create 10,000 fits for each of three biological replicates, randomly sampling a normal distribution (n=10,000) of v_C and v_A from control strain DL146. The mean and standard deviation of the fit ensemble were calculated as the mean and standard deviation differentiation and delay measures for each strain.

Supplementary Note 5. Estimating lysis rates from cytometry data

As described in Box 1 and the methods section, the lysis rate ρ for individual strains was estimated by applying parameter bootstrapping for growth rate, differentiation and delay estimates to fit Equations (5, 7) to the fraction of GFP-expressing altruists. Cytometry samples were processed as described in Supplementary Note 4.

An analytical solution to consumer and altruist populations that includes a lysis term and accounts for delayed differentiation as in Supplemental Equations S3 and S4 was generated from Equations (5, 7) of Box 1:

$$C(t) = e^{(v_C-\sigma)(t-\tau)}, \quad \text{(S3)}$$

$$A(t) = \frac{\sigma\left(e^{(v_A-\rho)(t-\tau)} - e^{(v_C-\sigma)(t-\tau)}\right)}{v_A - v_C - \rho + \sigma}. \quad \text{(S5)}$$

Lysis rate ρ was estimated from measurements of $\frac{A(t)}{A(t)+C(t)}$ fit to Equations (S3, S5) for the SDAc strains shown in Figure 2f (see Supplementary Table 4 for values). Fits and parameter bootstrapping were performed as described for differentiation rate estimates in Supplementary Note 4. Random growth rate estimates for bootstrapping were sampled from cellulase production variant DL147 and differentiation rates estimates were sampled from rates of the appropriate switch variant.

Supplementary Note 6. Estimating biomass yield for cellobiose and PASC

The Monod model of bacterial growth assumes a linear relationship between the saturated density of cells and the limiting nutrient and states that the slope of the line is the yield coefficient for the nutrient[4]. Here, we depict that relationship as

$$Y(n) = \gamma n + b, \quad \text{(S6)}$$

with Y as the biomass yield, γ as the yield coefficient, n as the nutrient level and b as an inoculation-dependent y. DL146 cultures grown in cellobiose appeared to be carbon limited only at concentrations below 1 g L^{-1} (Supplementary Figure 7a). When all cellobiose concentrations are included in the fit, carbon utilization matches an exponential saturation model,

$$Y(n) = S(1 - e^{\alpha n}), \quad \text{(S7)}$$

with *S* as the maximum biomass yield afforded by the limiting nutrient. No saturation was observed for PASC (Supplementary Figure 7b), suggesting the media remains carbon limited up to 4 g L^{-1}. Comparison of the slopes for each carbon source ($\gamma_{\text{PASC}}/\gamma_{\text{cellobiose}}$) suggests approximately 14% of available carbon in the cellulose is released in a digestible form for cellulase CelD04. Estimates for γ are summarized in Supplementary Table 6.

Supplementary Note 7. Estimating cellulase activity rates

Culture densities before and after sonication were used to estimate altruist concentration *A* and lysis efficiency ρ from Equation 3 of Box 1. As mentioned in the Methods section, two approaches were used to estimate cellulose hydrolysis: Congo Red staining of residual cellulose and biomass conversion from released nutrients. Congo Red absorbance measurements consistently suggested higher cellulose degradation rates than the nutrient release assay, suggesting some hydrolysis products, including oligomers larger than cellobiose, might not be digestible by SDAc strains.

A spectrophotometric calibration curve was established to estimate residual cellulose by measuring absorbance at 480 nm for PASC supernatant stained with 0.15% Congo Red. The calibration curve was generated for PASC concentrations from 2.68 g L^{-1} to 4 g L^{-1}. Absorbance readings were converted to cellulose concentrations using a linear fit to the calibration curve ($R^2 = 0.8869$).

$$[Cellulose] = -(0.595 \pm 0.0125) \times ABS_{480} + (4.7 \pm 0.03) \quad \text{(S8)}$$

Cellulose concentrations were estimated from released nutrients by measuring viable cell counts of cultures grown in PASC supernatant and converting cell counts to nutrients using the γ parameter and Supplementary Equation S6.

$$F = F_0 - n_i = F_0 - \frac{CFU(n_i) - b}{\gamma} = 0.004 - \frac{CFU(n_i) - (5.1\text{e}07 \pm 1.68\text{e}07)}{(1.28\text{e}12 \pm 3.34\text{e}10)} \quad \text{(S9)}$$

Parameter bootstrapping was used to estimate feedstock degradation for measurements using each method by generating mean and standard deviation statistics for 10,000 fits, each randomly sampling from a normal distribution of the error for the appropriate calibration curve.

An analytical solution to feedstock levels was generated from Equation (3) of Box 1 to estimate cellulase activity rates from Congo Red absorbance or nutrient release measurements,

$$F = Pe^{-\alpha\rho At} + f, \quad \text{(S10)}$$

with parameters *P*, α, and *f*. By the rules of derivation, the cellulase activity rate ω is the product of *P* and α. Fits were generated using initial altruist concentrations (*A*) and lysis efficiency (ρ) measured for each strain (Supplementary Table 7).

Supplementary Note 8. Estimating half-maximal rate constants for growth and differentiation

Nutrient-specific half-maximal rate constants for consumer and altruist growth – (k_C and k_A, respectively) and differentiation (k_σ) were fit to the growth curve for strain DL110. 10,000 fits were generated using parameter distributions with the mean and standard deviation for σ, ρ and ω associated with switch variant $(\mathrm{T})_{16}/(\mathrm{A})_{10}$, lysis rbSSR variant $(\mathrm{AT})_8$ and CelD04 payload variant from Supplementary Tables 4, 5 and 7, respectively. Parameter bootstrapping distributions for growth rates (v_C, v_A) were generated from DL147 (Supplementary Table 3):

$$\begin{aligned} v_C &= 0.459 \pm 0.004 \\ v_A &= 0.413 \pm 0.012 \\ \sigma &= 0.116 \pm 0.009 \\ \rho &= 0.191 \pm 0.025 \\ \gamma &= 1.279 * 10^{12} \pm 3.344 * 10^{10} \\ \omega &= 1.6 * 10^{-12} \pm 5.3 * 10^{-13} \end{aligned}$$

The half maximal constants for C and A are assumed to be the same and were fit as one parameter. The resulting parameter fits are shown in Supplementary Table 8. These half-maximal rate constants were adopted for use as necessary in models for SDAc strains.

Supplementary Note 9. Setting initial conditions for nutrients and population size for full dynamics model

SDAc system dynamics, both in the model and the physical implementation, were sensitive to initial conditions. For example, PASC growth media was inoculated with SDAc cultures directly from a saturated culture in rich media. Thus, the initial concentration of viable cells was dependent on differentiation rate (cultures with high differentiation rates likely generate more altruists, reducing the concentration of viable cells) and the inoculum included cellulase payload to begin converting PASC to nutrients. To account for these details, initial nutrients (with a concomitant reduction in initial feedstock) and initial population size were estimated as a function of the differentiation rate σ. Nutrients levels were estimated by fitting a logarithmic curve to the growth yield of DL146 in PASC media with filtered supernatant from SDAc strains DL046, DL112, DL110 and DL108, applying Equation 8 from Box 1 to convert CFUs to nutrients. Parameter bootstrapping from uncertainty in the γ parameter (Supplementary Equation S6) was applied to the fit (10,000 samples), which produced an estimate for initial nutrients as a function of differentiation rate: $n_0 = (1.952 * 10^{-4} \pm 2.952 * 10^{-5}) \log(\sigma) + (8.529 * 10^{-4} \pm 9.463 * 10^{-5})$.

A linear curve fit was used to map differentiation rate to initial population size. Viable cell count mean and standard deviation measurements from the same SDAc strains above were used to map differentiation rate σ to initial cell concentration x_0: $x_0 = -(1.7{\times}10^8 \pm 4.14{\times}10^7)\sigma + (3.66{\times}10^7 \pm 5.43{\times}10^6)$. Initial population estimates were distributed among consumers and altruists by applying the steady state solutions to Equations 5 and 6 from Box 1 for DL147 growth rates and strain-specific differentiation rates.

Supplementary Note 10. Estimating SDAc cheater rates

Cooperation escape rates for consumers and for altruists were estimated by applying parameter bootstrapping for growth, differentiation and lysis rates to fit Equations (9-12) from Box 1 to the fluorescence distribution data from SDAc strain DL108. The model was fit to the fluorescence distribution data (collected as described in Supplementary Note 4) separately with different assumptions: no cheaters ($\chi_C = \chi_A = 0$, simplifies to Equations 5-6), differentiation cheaters only ($\chi_A = 0$) and both differentiation and lysis cheaters. Cheater rates for the latter two assumptions are shown in Supplementary Table 9. The fits were generated using the Levenberg-Marquardt nonlinear least squares algorithm (nlsLM) in R.

Supplementary References

1. Bokinsky, G. *et al.* Synthesis of three advanced biofuels from ionic liquid-pretreated switchgrass using engineered Escherichia coli. *Proc Natl Acad Sci USA* **108,** 19949–19954 (2011).
2. Efron, B. & Tibshirani, R. Bootstrap methods for standard errors, confidence intervals, and other measures of statistical accuracy. *Statistical science* (1986). doi:10.2307/2245500
3. Egbert, R. G. & Klavins, E. Fine-tuning gene networks using simple sequence repeats. *Proc Natl Acad Sci USA* **109,** 16817–16822 (2012).
4. Monod, J. The growth of bacterial cultures. *Annual Reviews in Microbiology* (1949).